TALLINN UNIVERSITY OF TECHNOLOGY

SCHOOL OF ENGINEERING

Department of Materials and Environmental Technology

DEVELOPMENT OF SELENIUM MONOGRAIN LAYER SOLAR CELL

SELEEN-MONOTERAKIHT PÄIKESEPATAREI ARENDAMINE

MASTER THESIS

Student: Kaia Liisa Hakk

Student code: 204675KAYM

Supervisor: Dr. Taavi Raadik, Research Scientist

Dr. Mare Altosaar, Lead Specialist

Tallinn 2022

(On the reverse side of title page)

AUTHOR'S DECLARATION

Hereby I declare, that I have written this thesis independently.

No academic degree has been applied for based on this material. All works, major viewpoints and data of the other authors used in this thesis have been referenced.

".....” ..... 20…..

Author: .....

/signature /

Thesis is in accordance with terms and requirements

".....” ..... 20….

Supervisor: ….....

/signature/

Accepted for defence

".....”.....20… .

Chairman of theses defence commission: .....

/name and signature/

Non-exclusive licence for reproduction and publication of a graduation thesis[1]

I, Kaia Liisa Hakk

1. grant Tallinn University of Technology free licence (non-exclusive licence) for my thesis

"Preparation of selenium monograin layer solar cell"

supervised by Dr. Taavi Raadik and Dr. Mare Altosaar.

1.1 to be reproduced for the purposes of preservation and electronic publication of the graduation thesis, incl. to be entered in the digital collection of the library of Tallinn University of Technology until expiry of the term of copyright;

1.2 to be published via the web of Tallinn University of Technology, incl. to be entered in the digital collection of the library of Tallinn University of Technology until expiry of the term of copyright.

2. I am aware that the author also retains the rights specified in clause 1 of the non-exclusive licence.

I confirm that granting the non-exclusive licence does not infringe other persons' intellectual property rights, the rights arising from the Personal Data Protection Act or rights arising from other legislation.

_____ (date)

[1] *The non-exclusive licence is not valid during the validity of access restriction indicated in the student's application for restriction on access to the graduation thesis that has been signed by the school's dean, except in case of the university's right to reproduce the thesis for preservation purposes only. If a graduation thesis is based on the joint creative activity of two or more persons and the co-author(s) has/have not granted, by the set deadline, the student defending his/her graduation thesis consent to reproduce and publish the graduation thesis in compliance with clauses 1.1 and 1.2 of the non-exclusive licence, the non-exclusive license shall not be valid for the period.*

TalTech Department of Materials and Environmental Technology

THESIS TASK

Student: Kaia Liisa Hakk, 204675KAYM

Study programme: KAYM, Materials and processes in sustainable energetics

Main speciality: Materials in sustainable energetics

Supervisor(s): Dr. Taavi Raadik, Research Scientist, +3726203210

Dr. Mare Altosaar, Lead Specialist, +3726203362

Thesis topic:

(in English) Preparation of selenium monograin layer solar cell

(in Estonian) Seleen-monoterakiht päikeseelemendi valmistamine

Thesis main objectives:

1. Determining the preparation conditions for selenium monograins
2. Characterising the properties of prepared monograins for use in monograin layer solar cell
3. Testing of selenium monograin layer solar cell

Thesis tasks and time schedule:

No	Task description	Deadline
1.	Preparation of selenium microcrystals for phase transition, using different heating methods	20.12.2020
2.	Preparation and deposition of ZnMgO layer	09.02.2021

3.	Finishing selenium monograin layer solar cell and testing	08.06.2021
4.	Writing the thesis	23.05.2022

Language: English **Deadline for submission of thesis:** 22.05.2022

Student: Kaia Liisa Hakk 22.05.2022

/signature/

Supervisor: Dr. Taavi Raadik …….. "....."..... 20….a

/signature/

Consultant: …… …..... "....."..... 20….a

/signature/

Head of study programme: Dr. Sergei Bereznev ..... "....."..... 20…..a

/signature/

Terms of thesis closed defence and/or restricted access conditions to be formulated on the reverse side

CONTENTS

PREFACE 8

List of abbreviations and symbols 9

INTRODUCTION 10

1 THEORY AND LITERATURE REVIEW 12

1.1 Fundamentals of solar cell 13

1.1.1 Absorber materials in solar cells 16

1.1.2 Selenium (Se) as an absorber material and its properties 16

1.2 Monograin technology 18

1.3 Summary of literature review and aim of the study 20

2 EXPERIMENTAL 22

2.1 Preparation of Selenium grains 22

2.1.1 Heating in a tube furnace 24

2.1.2 Heating in a muffle furnace 26

2.1.3 Heating in solid potassium iodide (KI) 28

2.2 Deposition of *n*-type buffer layer and completing MGL solar cell 29

2.2.1 Deposition of ZnMgO buffer layer 30

2.3 Characterization of microcrystals and ZnMgO layers 31

2.3.1 Raman spectrometry 31

2.3.2 Scanning electron microscopy (SEM) 32

2.3.3 Sieving 32

2.4 Solar cell characteristics 33

2.4.1 Current-Voltage measurements 33

2.4.2 Quantum efficiency measurements 34

3 RESULTS AND DISCUSSION 36

3.1 Morphology of selenium microcrystals 36

3.2 Phase composition of Se 39

3.3 ZnMgO layer deposition 41

3.3.1 Chemical composition of solution for ZnMgO deposition 41

3.3.2 Deposition process 42

3.3.3 Deposition of ZnMgO on ITO and FTO 45

3.3.4 Deposition of ZnMgO on Se membrane 46

3.4 Solar cell 47

SUMMARY 52

KOKKUVÕTE 54

LIST OF REFERENCES 56

PREFACE

Topic for this thesis was initiated by my supervisor, research scientist Dr. Taavi Raadik. The focus of this research is to gain better understanding of selenium as a promising material for monograin layer solar cell. Experimental work was carried out in Tallinn University of Technology at the Department of Materials and Environmental Technology, Laboratory of Photovoltaic Materials.

I would like to show my gratitude to my supervisors, research scientists Dr. Taavi Raadik and Dr. Mare Altosaar who gave me advice and support during the experimental and theoretical parts of the work. Moreover, I would like to thank the staff of mentioned laboratories that contributed their knowledge towards my topic. They are Dr. Maris Pilvet, Dr. Jelena Maricheva, Dr. Valdek Mikli and PhD student Katriin Kristmann. Finally, I would like to thank the head of Laboratory of Photovoltaic Materials Dr. Marit Kauk-Kuusik for opportunities to conduct the work in the lab.

In this paper, the main focus is on creating selenium microcrystals suitable for photovoltaic purposes. In addition, deposition of ZnMgO layer as a buffer layer for selenium monograin layer solar cell is described in detail. The latter part composes of completing a solar cell and testing of this element.

The study was financially supported by the Estonian Research Council project PRG1023, by ERDF project „Center of nanomaterials technologies and research (NAMUR+)" (2020.4.01.16-0123), by the European Union through the European Regional Development Fund, Project TK141 and by European Union's H2020 research and innovation programme under Grant Agreement No. 952982.

Keywords: Selenium, ZnMgO, monograin layer solar cell, Master thesis.

List of abbreviations and symbols

CBD	chemical bath deposition
E_g	band gap
EQE	external quantum efficiency
FF	fill factor
I_{MP}	maximum point current
I_{SC}	short-circuit current
ITO	indium tin oxide
J_{sc}	short-circuit current density
MGL	monograin layer
MPP	maximum power point
η	efficiency
PCE	power conversion efficiency
PV	photovoltaics
SEM	scanning electron microscopy
V_{MP}	maximum point voltage
V_{oc}	open-circuit voltage

INTRODUCTION

The global energy system is mainly based on fossil fuels that are non-renewable and emit high levels of greenhouse gases. We are already seeing the impacts to the environment such as earth average temperature rise. To change the course of this route, countries are already switching their focus towards renewable energy. But this transformation is an extremely high-scale one, and we are still at the very beginning of it all.

With the growth of world's population and increasing use of technology, there is an increase in electricity demand and it is expected to reach to the 50 TW for 2050. Renewable energy sources have been gaining more and more attention as the world needs an alternative to fossil fuels, especially now where the world has entered to the worldwide energy crisis. Their energy is gained from continuous or repeating events in the natural environment. [1] Fossil fuels emit greenhouse gases and their sources are non-renewable.

The European Union has set a united goal to lower greenhouse gas emissions by 80-95% by 2050. [2] That could be compared to pre-industrial times. Initial goal was reviewed in 2020 and it was concluded that the target was too ambitious. Even though this high percentage is unreachable at this moment in time, EU will still move towards reducing emissions by at least 40% by 2050. It is also predicted that by the same year renewables could make up 60% or more of the total energy consumption for many countries. [2] Integrating photovoltaic systems into the grid has multiple strong arguments. Solar arrays can be built in multiple sizes, from small scale (residential houses) to large scale (solar parks), they can be distributed all over the country, by doing this ensuring the energy security. When installed correctly, they require little maintenance and produce electricity without polluting the environment. [3] Despite the fact that the commercial solar cells have been on the market around 70 years, there is still continuous work on finding more abundant, environmentally friendly and cost-effective solar cell materials.

In this research study, selenium microcrystals are studied as an absorber material for monograin layer solar cell. Selenium is the first semiconductor material used to construct a photovoltaic element, but despite that its efficiency pales next to other materials such as silicon. [4] It has good absorption coefficient, suitable bandgap and low melting temperature, all this make selenium very attractive absorber material for a solar cell. In addition, selenium is abundant in the Earth's crust and is a non-toxic material.

Current thesis is focused on the experimental work carried out in Tallinn University of Technology at the Department of Materials and Environmental Technology, Laboratory of Photovoltaic Materials.

1 THEORY AND LITERATURE REVIEW

Although the Sun is tremendously powerful energy source and most abundant received by Earth, its intensity on the ground is quite low. About 54% of the incoming sunlight is scattered or absorbed by clouds and atmosphere. That being said, our planet still receives nearly 10 000 times the energy required daily. [1] The amount of solar energy varies due to factors such as geographic location, time, season, weather. If collected, this can be turned into useful form of energy – electricity and/or heat. [5]

Among the alternative sources, solar energy is the largest one. Photovoltaic (PV) solar energy production has been in the focus of research and most studied. The energy production from sunlight is considered to be clean and does not produce noise. [6] Although in recent years the usage of solar energy has been growing exponentially there is still room for new emerging and cheap photovoltaic technology to cover world energy demand in the future. In Figure 1.1, a diagram consisting of renewable energy sources is presented. This is the forecast of market share, in percentages, for 2022-2027. It could be seen that solar energy has the potential to cover over half of forementioned market.

Figure 1.1. Global renewable energy market share forecast 2022-2027, % [7]

In the following chapters, the working principle of a solar cell and an overview of selenium and its properties is presented. It will also cover what are monograin layer (MGL) solar cells.

1.1 Fundamentals of solar cell

Solar cells' working principle is based on the photovoltaic (PV) effect. PV effect was firstly experimentally demonstrated by Edmund Becquerel in 1839 and explained theoretically by Albert Einstein in 1905. [1] For the theoretical description of PV effect A. Einstein received Nobel Prize in Physics in 1921. In short, the PV effect can be described by phenomena where light interacts with matter and, as a result electrons are made free to move within the semiconductor. In a wide scale, there are three types of materials – insulators (for example: rubber), semiconductors and conductors (for example: metals). In an insulator all electrons are bonded tightly, without freedom to move in a crystal lattice. In a conductor, electrons at higher energy levels can freely move around, making them conduction electrons. A semiconductor is a solid material where there are bonded electrons within an energy zone, called valence band, and free electrons above a certain energy value. In between those, there is an energy band gap forbidden for electrons. What makes a semiconductor special is the fact that its' bandgap has a value that allows to modify the amount of electrons in its conduction band by changing some parameters (temperature, composition, electric field, excitation with light etc). Difference between those materials is illustrated in Figure 1.2. [6], [8]

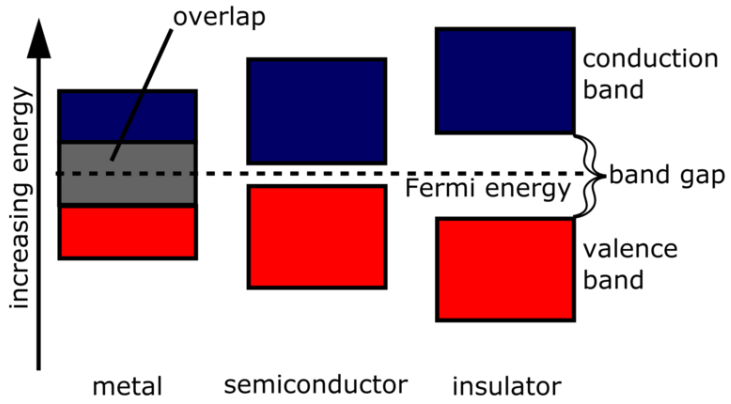

Figure 1.2. Difference in band gap values for insulators, semiconductors and conductors [8]

Energy value of a band gap (E_g) is the minimal amount of energy to excite an electron from valence band to conduction band. Fermi energy is an energy level where the statistic probability of holes and electrons is even. When the electron reaches conduction band, a hole in the valence band is left. *Vice versa*, an electron in the conduction band can lose its energy and fall back into valence band. An electron from a nearby atom can fill this space, creating a continuous reaction. A hole is treated as a positive charge carrier and an electron as a negative one. [6],[8] There are two types of semiconductors - *p*-type where material has a high hole concentration and *n*-type that has a high

electron concentration. If we drive these two different types of semiconductors in a contact, a *p*-*n* junction is created which is a base for most of the optoelectronic devices. [6], [9] In Figure 1.3 a process of *p*-*n* junction formation is presented. A difference in concentrations of electrons (*n*) and holes (*p*) in two different types of materials is the driving force in these materials and it forces electrons to diffuse to *p*-side and holes towards *n*-side due to this. When the free carriers have diffused, an area of fixed charges remains. An electric field in that region pushes out the free carriers, making it the depletion region. [10]-[12]

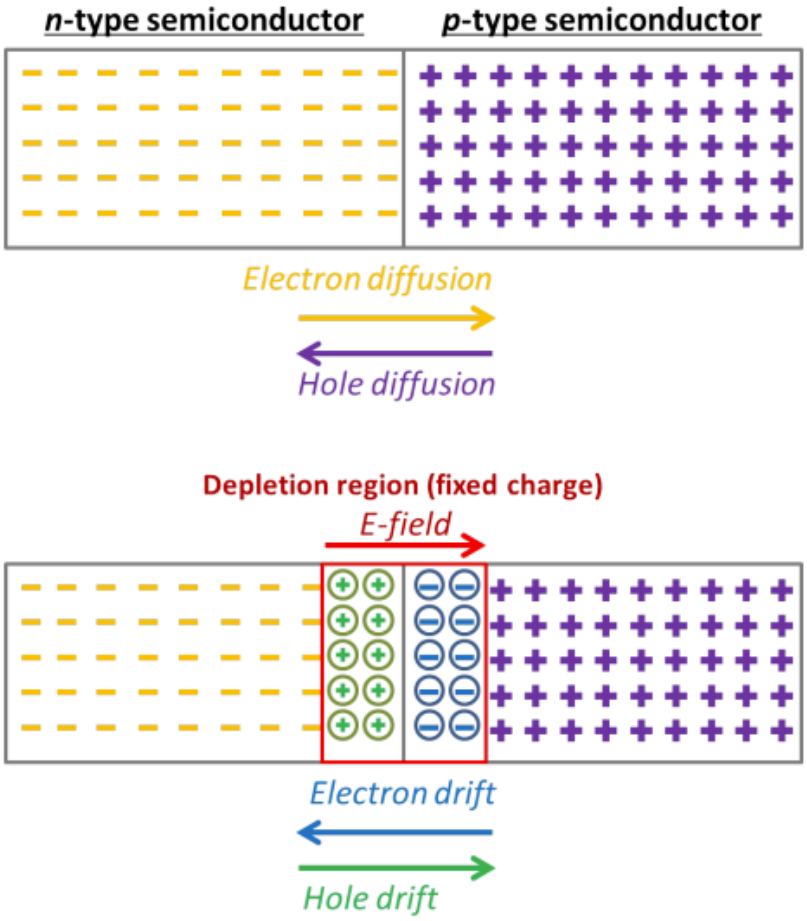

Figure 1.3. Formation of *p*-*n* junction [11]

A *p*–*n* junction can be formed also inside a single crystal of semiconductor. *p*–*n* junctions in solar cells work as diodes, it means as circuit elements that allow a flow of electricity in one direction but not in the other (opposite) direction. Therefore, electric field in *p*-*n* junction enables the electrons excited by light to enter to the outer electrical circuit.

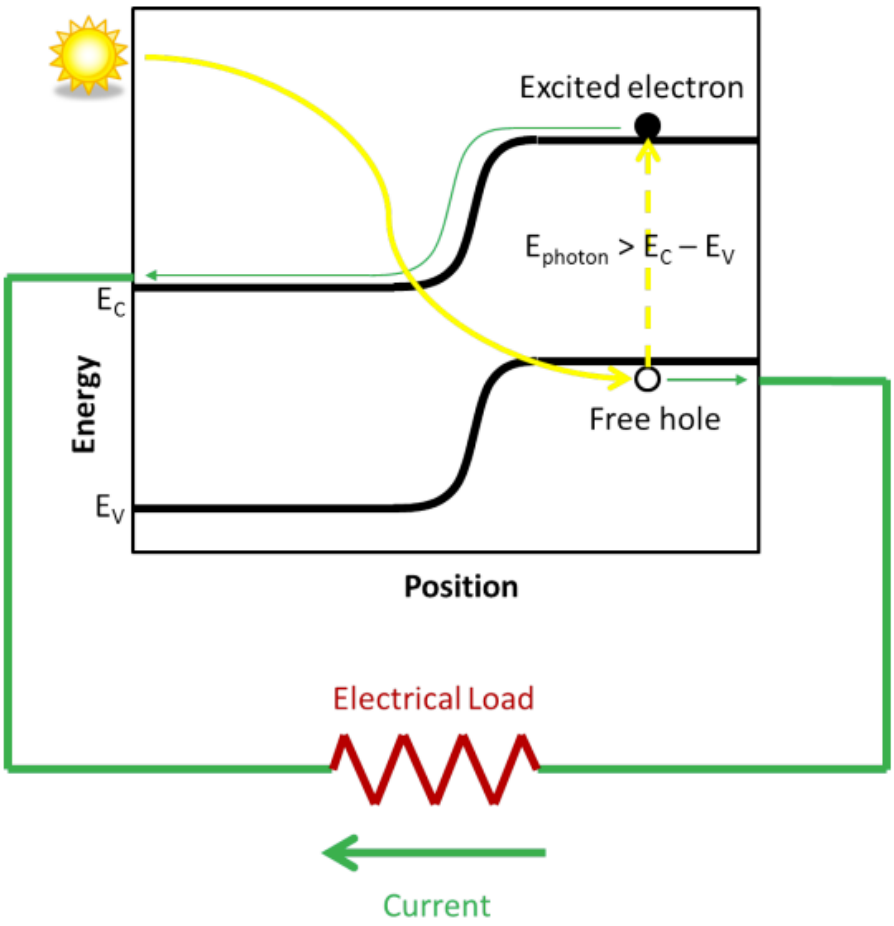

Figure 1.4. Solar cell operation [11]

The basics of a solar cell working principle is shown in Figure 1.4. Absorption of a light photon with energy greater than the band gap is how electrons can be excited from the valence band to the conduction band. If the energy is greater than E_g, the excess energy is released as heat. If it is lesser than E_g, it is not enough to excite the electron. When the energy reaching the solar cell is sufficient, an electron will be excited from the valence band to the conduction band and leave behind a free hole. This is called an electron-hole pair. The pair is separated when atoms are excited with radiant energy, in a semiconductor that is a part of a *p*-*n* junction and connected to an electrical load. Then the net flow of electrons start moving towards the contact on the *n*-type junction and *vice versa,* due to the electric field in depletion region, electrons towards *p*-type side, creating a current. [11]

Photovoltaic technology has been growing rapidly since it was discovered and now there are already three generations of solar cells. Selenium was the first semiconductor to be used as an absorber layer in a solar cell mock-up. This was also the basis of the photoconductivity characteristic observation years before. Since 1950s, the solar cell

materials have seen a wide range of discoveries and developments. Most widely used photovoltaic elements are still silicon-based. New technologies are reaching higher efficiencies than ever before. Although most of them are still in development phases, the future looks bright for solar energy.

1.1.1 Absorber materials in solar cells

In solar cells, an absorber layer is where the light is absorbed and an electron-hole pair is generated. Light can release an electron from its atomic bond at a certain energy (band gap) that is specific to the material and its atomic structure. This is usually displayed in electronvolts (eV). For a semiconductor material to be suitable as an absorber material, it's band gap would ideally be in the range of E_g=0.9-1.5 eV. [13] Silicon, as most widely used and known semiconductor, has a band gap of 1.1 eV. [3], [14]

Solar cells can be divided into three generations: wafer-based, thin film technology and emerging technology solar cells.

First generation is made of silicon wafers. There are mono-crystalline and poly-crystalline silicon solar cells. While mono-crystalline has higher efficiency, due to its high level of purity, it is expensive. In contrast, poly-crystalline silicon has lower efficiency, but also lower price. This generation is most widely explored at this moment in time. [13]

Second generation belongs to thin film technologies. Since they use less material, they could be considered as more economically efficient and they contribute less waste. Materials such as CdTe, GaSe, CIGS are excellent for this application. However, Cd is a toxic substance and therefore its usage is limited. [13]

The latest emerging technology include organic, perovskite, tandem, dye-sensitized and CZTS solar cells, for example. All of the mentioned technologies are said to be emerging because most of them are still in research phases and have yet to reach commercial use. While these photovoltaic absorber materials show high efficiencies, there is a problem with the stability of the cells. One of the issues is that organic materials tend to degrade over time. [13], [15]

1.1.2 Selenium (Se) as an absorber material and its properties

Selenium is an abundant element in the Earth crust. [6] The creation of selenium based solid-state solar cell initiated the research related to photovoltaics and gave initial

understanding into photoelectric effect that influenced Einstein's Nobel Prize. Selenium's photoconductivity was detected in 1873 when Willoughby Smith noticed that when Se was exposed to light, the current changed. He also observed that the current depended on the intensity of light. First large-scale solar cell was produced in 1894 by Charles Fritts. In this mentioned cell, selenium was sandwiched between gold and a sheet of another metal. [4], [5]

Research regarding selenium as an absorber material declined when no significant discoveries regarding solar cell application did not surface, and the increasing silicon market took over, leaving Se behind. First experiments with selenium solar cell showed efficiency below 1%, 5% was achieved in 1985 and the highest efficiency so far – 6.5% was achieved in 2017 [4]. This record efficiency of Se solar cell is far behind in comparison to rapidly growing silicon market (6% in 1954, 26.7% in 2018) [16]. In addition to silicon solar cells, new materials such as CIGSe, CdTe, GaAs, GaTe etc. started showing higher efficiency. [5], [6]

Now selenium is mostly used in tandem solar cell devices as a high bandgap counterpart material. Theoretical maximum of selenium solar cell is over 20%, which is why it revived the scientists' interest and is being researched more in depth now. [7]

Trigonal selenium is a light-Sensitive semiconductor material and has great stability in humidity and oxygen. The melting point of Se is around 220 °C, [19] meaning the substance can be processed at relatively low temperatures. The production costs for making trigonal selenium are low compared to other materials used in solar cell absorber layer. [6] For Se, to be suitable for a single element PV absorber, it needs to have the trigonal crystal structure (*t-Se*), it means to go thoroughly a crystallization process where amorphous selenium (*a-Se*) is transformed into trigonal selenium (*t-Se*). Selenium in this phase is composed of helical infinite Se chains that are arranged in a hexagonal lattice as shown in Figure 1.5. [3], [4]

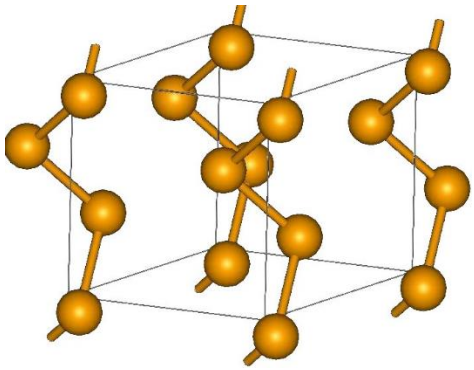

Figure 1.5. Crystal structure of trigonal selenium [20]

Trigonal selenium has a band gap in the range of 1.83-2 eV, depending on the fabrication technique, high absorption coefficient (over 10^{-4} cm^{-1}) and long charge carrier lifetime. [4] Additionally to the conventional single junction solar cell structure, selenium is an attractive candidate for tandem devices in the role of high bandgap layer, as was mentioned before. [6]

Previous studies [4] have shown that the time period for crystallisation of *a-Se* to *t-Se* structure is extremely important. Fast process resulted in random orientations such as in *a-Se* while slow crystallisation allowed the Se grains to orient and grow as homogenous. Transition from amorphous to trigonal starts at around 100 °C and growth rate peaks at around 185 °C from where on the speed of growth decreases. From this knowledge it could be concluded that the lower the annealing temperature, the smaller are the grains. At higher temperatures there could be a loss of orientation inside the grains. The study indicates that the grains with the best quality could be obtained at an optimum temperature where high orientation and size of the grains are in balance. [4]

1.2 Monograin technology

Solar cells today are mainly produced using mono- or polycrystalline silicon or thin film technologies. Aforementioned two silicon solar cell production methods use huge ingots that have high chemical purity. The ingots are sawn into thin wafers. This leads to an extensive loss of material reaching as high as 50%. Thin-film technology is used as an alternative, but the parameters of this type of solar cells are lower than those of monocrystalline technology. [18], [21] Solar cells developed on the base of powder materials are emerging and showing improved results. The monograin powder technology allows to grow grains that have single-crystalline structure, possess excellent crystallinity, such as single crystal silicon but uses only the fraction of material. [22]

Monograin layer (MGL) is a phrase that came into the field more than 40 years ago. It is a layer of grains where each has a single-crystalline structure and specific granulometric composition. The idea of the MGL design is valuable in the possibility to combine the high photoelectronic parameters of monocrystals and good assets of polycrystals like low cost, simple technology, using 100% of initial material and possibility to make flexible devices with cheap and reliable roll-to-roll production technique. [22] Synthesis-growth of initial powder particles in isothermal conditions in

molten solvents (inorganic salt fluxes) has proven to be a sufficient method to achieve improved crystal structure and reduced concentration of intergranular defects. [23]

Structure of a MGL solar cell is brought out in Figure 1.6 and it is as follows: back contact/ epoxy resin/ *p*-type monograin layer/ n-type buffer layer/ i:ZnO/ conductive ZnO/ glass. The monograins are submerged in epoxy to fix them in place inside the membrane. *N*-type buffer layer is then deposited on top of the MGL, typically by chemical bath deposition (CBD). Then the following layers (intrinsic and conductive ZnO) are set on top of each other. After gluing the structure onto supportive transparent front cover (glass plate or cover foil), the back side of crystals is released from epoxy by abrasive treatment with abrasive paper, so that the crystals are partly uncovered to attain contact, The structure is called as monograin membrane or monograin layer (MGL). [24]

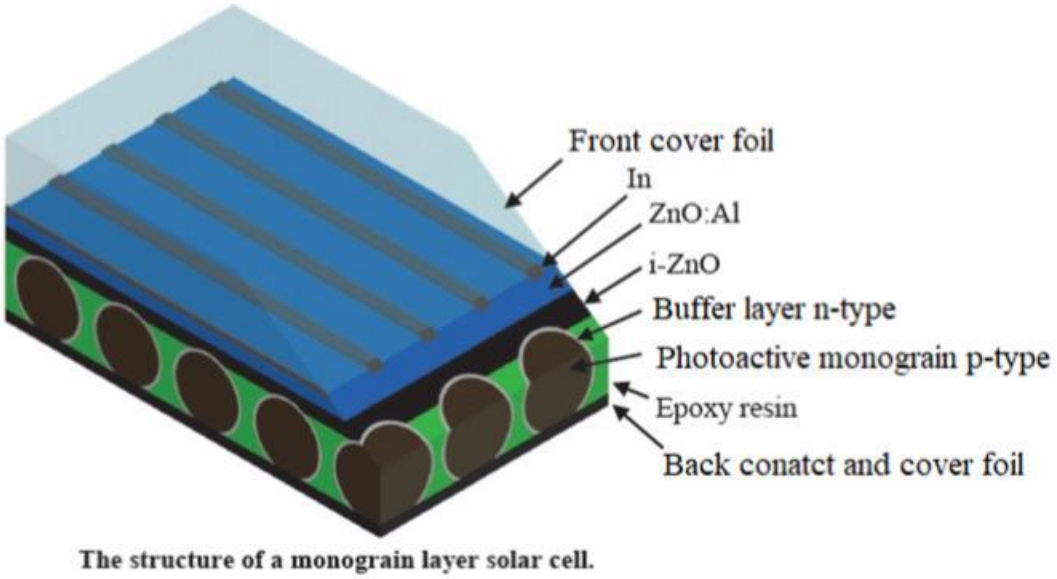

Figure 1.6. Structure of MGL solar cell [25]

In this study, the concept of MGL solar cell is used for making MGL absorber layers from selenium grains. For achieving *t-Se* structure the initial amorphous Se grains are recrystallized by annealing. For this, the sieved grains are spread as sparsely as possible onto a plate and annealed at different temperatures between 210 °C and 250 °C for different times and cooled down slowly to achieve the best grain morphological structure and uniform size. [18]

1.3 Summary of literature review and aim of the study

Solar energy has been gaining attention as an alternative energy source and its usage has been growing rapidly. Solar panels (PV elements) can be built in multiple sizes for specific applications and use the available source - the Sun. With rising need, new and highly efficient technologies are emerging. In contrast to first generation silicon solar cell, we are already seeing a third one – organic solar cells. Since these new alternatives are still in development, they do not see massive commercial use. Second generation thin film solar cells however are evolving fast. But these materials are expensive compared to silicon, for example. Some substances can also be hazardous or toxic to humans or to the environment. Researching a new approach that is less costly but more environmentally friendly is where the field should be headed.

Selenium is the first material that was used in creating a solar cell, but due to its slow evolution (below 1%, 5% in 1985 6.5% in 2017), it has been put on the back-burner. But it has a lot of suitable characteristics for a solar cell absorber layer.

Se is an abundant element on the Earth. It has a low melting temperature, suitable bandgap (1.83-2 eV) and long charge carrier lifetime. For selenium to be suitable as an absorber material, it needs to go through a crystallisation process, where *a-Se* is transformed into *t-Se*. Temperature and time are extremely important when it comes to this step. This determines whether microcrystals with random or homogenous grain orientation are produced.

Monograin layer solar cell consists of a layer of grains where each has a single-crystalline structure. In this method, nearly 100% of initial material is used which means that the waste is minimal. Most widely used way is to grow grains in molten solvents.

Aim of the study was formation of trigonal structure selenium microcrystals and use them as absorber material in the monograin layer solar cell. To achieve this:

- Selenium properties were analysed. Based on previous studies and research, the transformation of *a-Se* to *t-Se* was carried out using different methods to achieve best result.
- *N*-type ZnMgO buffer layer deposition methodology was studied and tested, before depositing it on a Se MGL membrane.

- The layers are characterised using optical microscopy, Raman Spectrometry and Scanning Electron Microscopy. The completed solar cell was tested and analysed with I-V measurements and Quantum Efficiency measurements.

2 EXPERIMENTAL

In this study selenium grains were thermally treated to achieve recrystallized microcrystals using a - tube furnace or a muffle furnace. To avoid the contacting of the grains with each other, in some tests, solid KI was used to keep the initial particles separately. First, the two aforementioned methods were performed on a plate while the last in quartz ampoules. To achieve the best morphology and crystallinity of grains for solar cell use, different heat-treatment times and temperatures were tested.

In the second part, ZnMgO buffer layer deposition was studied in order to finish monograin layer solar cell. ZnMgO was chosen as *n*-type partner because it was used in the record 6.5% PCE Se solar cell. [14] Recipes for ZnMgO were varied and the deposition regimes were tested multiply to achieve the continuous and even well covering film.

2.1 Preparation of Selenium grains

Preparation of a selenium solar cell started with the production of *t-Se* grains. Grinding of Se precursor material was done in an agate mortar to achieve small pieces of selenium. Grinding was done inside a plastic bag to avoid contamination. Initial selenium pellet (seen in Figure 2.1, right) was with a diameter around 4-5 mm. On the left image is shown the bottle in where the pellets resided.

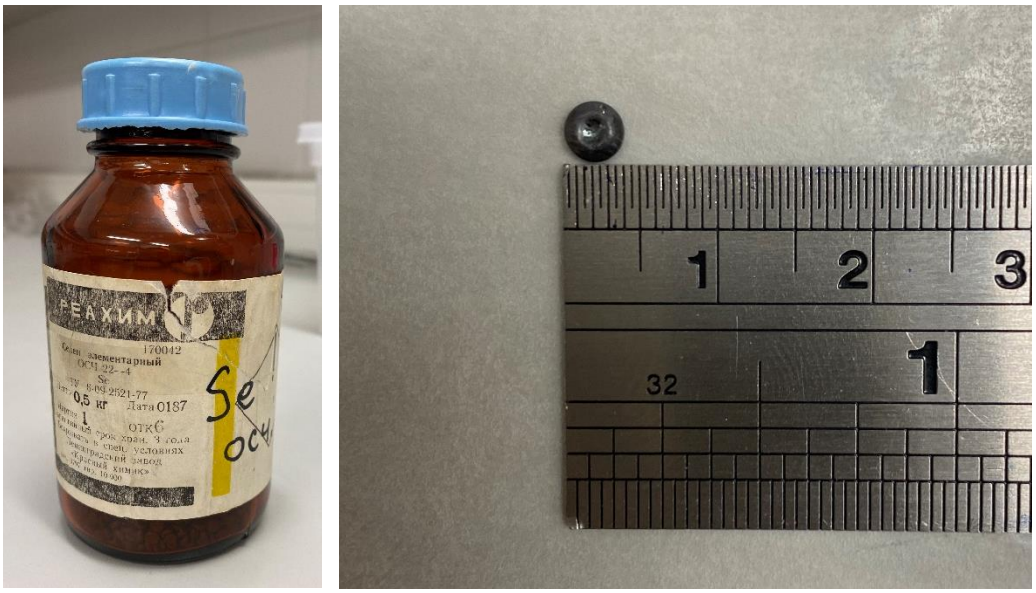

Figure 2.1. Left: Bottle with Selenium precursor material; right: selenium granule

For further understanding the characteristics of precursor selenium, differential thermal calorimetric measurements were performed in a vacuum sealed ampoule. Se melting temperature is around 221 °C. [19] In Figure 2.2, there can be seen almost unnoticeable thermal effect at around 185 °C, referring to growth rate peak and probably belonging to the phase transformation. The endothermic peak starting in around 219 °C indicates that selenium granules were melting at that temperature. As the calorimetric analysis result matches the references, in upcoming experiments this knowledge was taken as a reference for choosing the furnace temperature regimes.

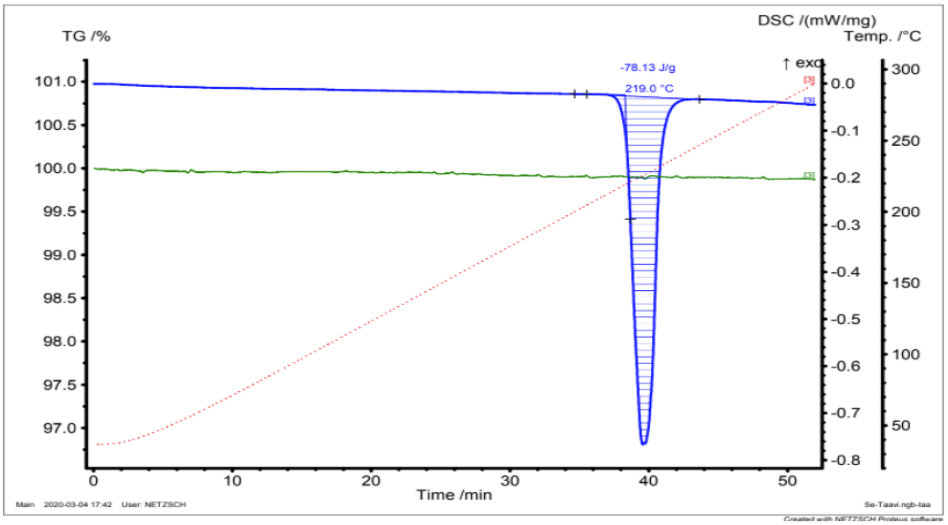

Figure 2.2. Differential calorimetric analysis curve of selenium

The recrystallisation of selenium pieces into microcrystals was proceeded using 3 different methods: in a tube furnace in nitrogen or argon gas environment, one zone furnace and in ampoules where Se particles were mixed with solid potassium iodide.

2.1.1 Heating in a tube furnace

The grinded and usable fraction of 63-75 μm sieved Selenium grains were placed on a sample plate that was previously soot covered by scorching. To avoid the grains sticking together during the melting process, it was important to scatter the grains. Due to the narrow furnace tube, the plate was in a size of 5x5 cm and fit around 1000 microparticles. Microcrystals were scattered by hand on a plate as presented on Figure 2.3.

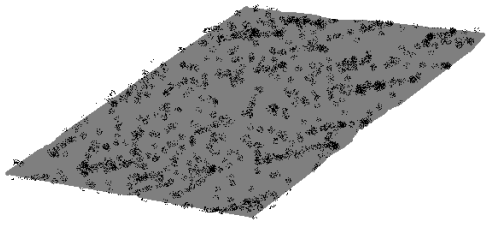

Figure 2.3. Se microparticles scattered on a plate

Three-zone furnace is a heating system which can be used to heat three zones (left, center, right) at different temperatures. On upper image in Figure 2.4 there is presented a three-zone furnace that is in the lab of solar cell materials technology of TalTech. Since during the current experimental work only one single sample was placed into the central zone, the left and right zones had the same heating program (temperature profiles) as the central zone. Lower image in Figure 2.4 shows how the sample was placed inside the system. The plate was placed on top of a base to stabilize the plate and prevent it from falling. It also made it easier to push the plate into the center of zone. The furnace enables the user to control the process temperature, as well as the environment, so the experiments can be done in vacuum environment or in a gas flow (nitrogen, argon). In current experiment, the positive pressure was kept in the furnace with the gas flow that prevents selenium microcrystals from evaporating.

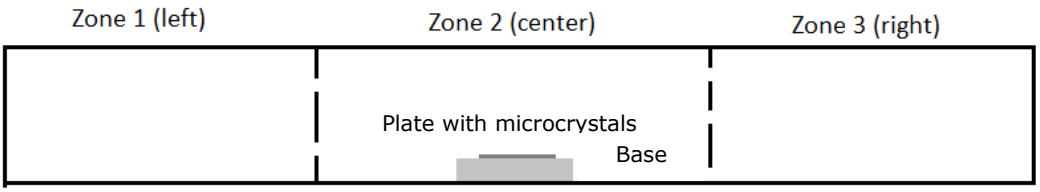

Figure 2.4. Up: Overview of the three-zone furnace used for heat treatment of Se samples at TalTech; Down: Sample's position inside the three-zone furnace

To achieve the best result (morphology, structure), multiple oven regimes were tested. Main parameters changed during each testing phase were the heating temperature and cooling time. For heating temperature, it was important for it to be high enough so that selenium will start to melt. Cooling time followed and it determined the phase transformation of the microcrystals. Figure 2.5 presents the heating profile of the first successful selenium grain crystallisations. The furnace was heated up to 225 °C and then cooled down to 200 °C in 180 minutes. After this, linear cooling to room temperature was set.

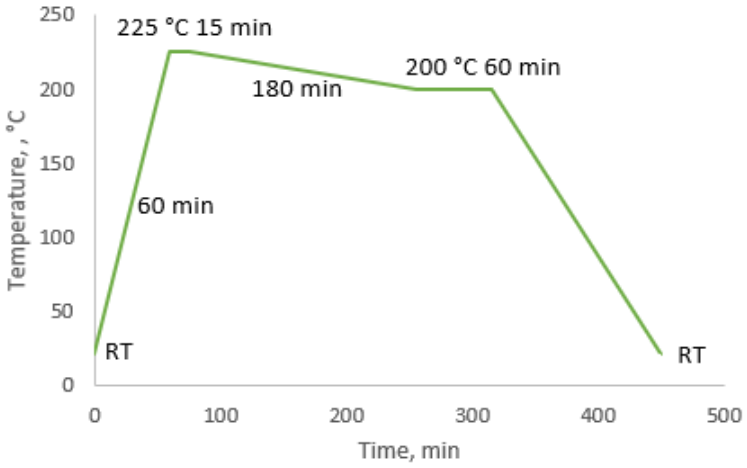

Figure 2.5. Heating profile for crystallization in three-zone furnace

2.1.2 Heating in a muffle furnace

In addition to the crystallisation in three-zone furnace, a muffle furnace was used. A photo of the furnace used for selenium crystallisation is presented in Figure 2.6.

Figure 2.6. Furnace used for selenium crystallisation

To get a better overview of difference between showed temperature and actual temperature inside the muffle furnace, a measurement was carried out. The result is seen in Figure 2.7. When setting the oven scheme for crystallisation process, this was used to achieve the most accurate temperatures.

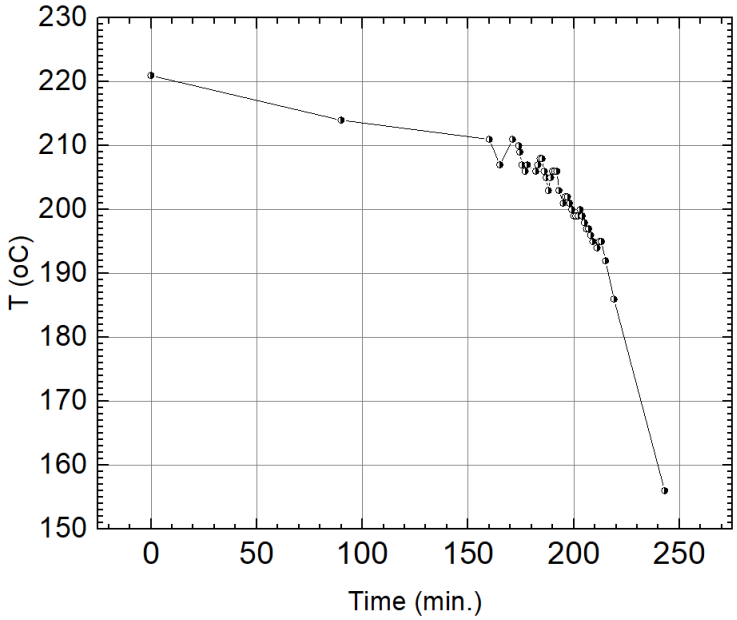

Figure 2.7. Measured cooling curve of muffle furnace

In Figure 2.8, there is depicted a mock-up of test organization how the selenium microcrystals were placed inside the furnace. The plate with selenium pieces on it was covered with a glass dome to prevent fast Se sublimation and contamination of the furnace chamber with selenium deposits and finally, to avoid the microcrystals from „flying away" from the plate.

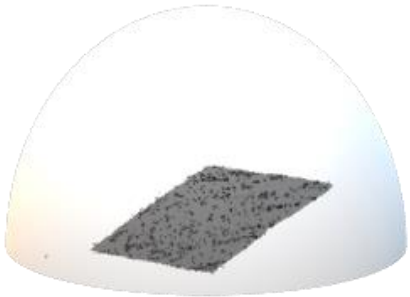

Figure 2.8. Plate of Se microcrystals under a dome

2.1.3 Heating in solid potassium iodide (KI)

While the heating processes for three-zone furnace and muffle furnace were showing expected results, it only allowed the fabrication of microcrystals in very small amounts. That is why a third method, heating in an ampoule, was looked into. Chosen solid potassium iodide (KI) was mixed with Se particles and the mixture was mounted into an ampoule. The mass ratio of KI to selenium was 2:1. The idea of the process was to surround selenium particles with crystals of KI that would border Se microparticles and keep them apart from each other. In Figure 2.9, a photo of an ampoule is presented. Inside it, selenium microcrystals and KI are mounted. Magnification in the same figure shows how the explanation mentioned before would look like. When reaching melting temperature of selenium, KI particles surrounding Se grain would help the grain to keep its spherical shape and avoid melting together. This was an attempt to avoid the microcrystals from creating bundles.

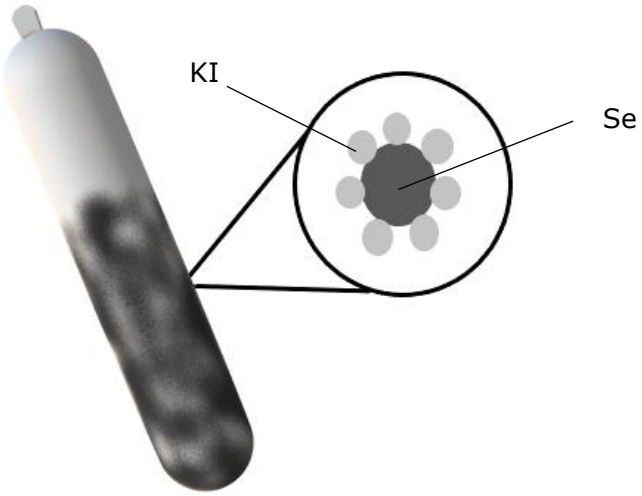

Figure 2.9. Se in KI inside an ampoule

In Figure 2.10, there is presented the temperature profile of Se heating in the presence of solid powdery KI. Since the same scheme was used in previous two heating processes, the temperature/time markings are similar to previous crystallisation schemes. Microcrystals were heated up to 250 °C, stabilized for 300 minutes. Then the temperature was decreased to 220 °C and kept there for an hour. After this natural cooling took place.

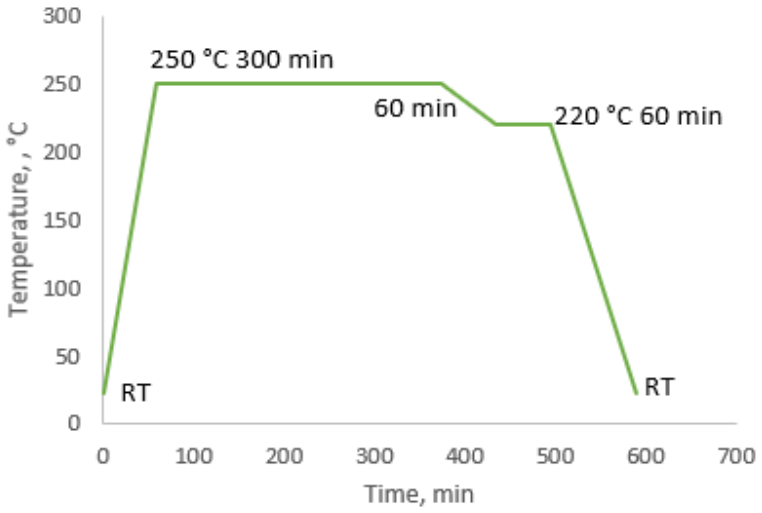

Figure 2.10. Scheme for selenium crystallization in KI

2.2 Deposition of *n*-type buffer layer and completing MGL solar cell

In order to prepare a monograin layer membrane as the base for the solar cell structure, sieving of Se powder particles was done and the 63-75 μm size fraction of selenium microcrystals was sorted out. Sieved powder particles were inserted into a thin layer of polymer with thickness of 20 microns, that was applied to the polymer film with applicator, the way that upper surface of grains was outside the polymer and the monograin layer membrane was formed.

The buffer layer was deposited on top of the monograin layer membrane, followed by RF sputtered i:ZnO and Al doped ZnO as a front conductive oxide for a charge collection.

After the solar cell had all the necessary layers, back contact needed to be brought forward to ease the process of testing later on. At first, the subject is etched in H_2SO_4 for 15 seconds. Then, taking a piece of sandpaper, polishing is next. Goal is to unveil the selenium grains evenly to create contact. To make sure the grains are visible, an optical microscope was used. If they needed more etching and polishing, this process was repeated until all the Se crystals were opened from epoxy,

When the etching stage was completed, it was time to apply contacts on the cell. For this, graphite paste was used. On the membrane, there was space for 4 spherical graphite contacts with diameter of 4 mm. *I-V* curves were measured, showing whether

the cell produced energy. In an attempt to further improve the result, graphite was substituted with vacuum deposited gold contacts.

2.2.1 Deposition of ZnMgO buffer layer

At first, CdS was deposited on the selenium grains. The resultant SEM images showed an inconsistent non-homogenous layer. Due to this reason, for the selenium MGL solar cell prepared in this study, ZnMgO was chosen as the *n*-type buffer layer. Since it was possible to produce the recrystallized Se microcrystals in a small amount at a time, the first tests to deposit ZnMgO layers were done on conductive FTO and ITO glasses. When the ratios and order were set, ZnMgO was deposited onto a selenium microcrystal membrane.

ZnMgO is a new type of material that emits light in the ultraviolet spectrum and has potential applications in optoelectronic devices such as photovoltaic elements. ZnO has a wurtzite structure while MgO has halite (cubic) structure. In Figure 2.11, there is presented the phase diagram of ZnMgO on temperature 800-2000 °C. Even though the experiments carried out in a temperature below this, it could be concluded that the desired phase for solar cell usage is wurtzite + halite. [26], [27]

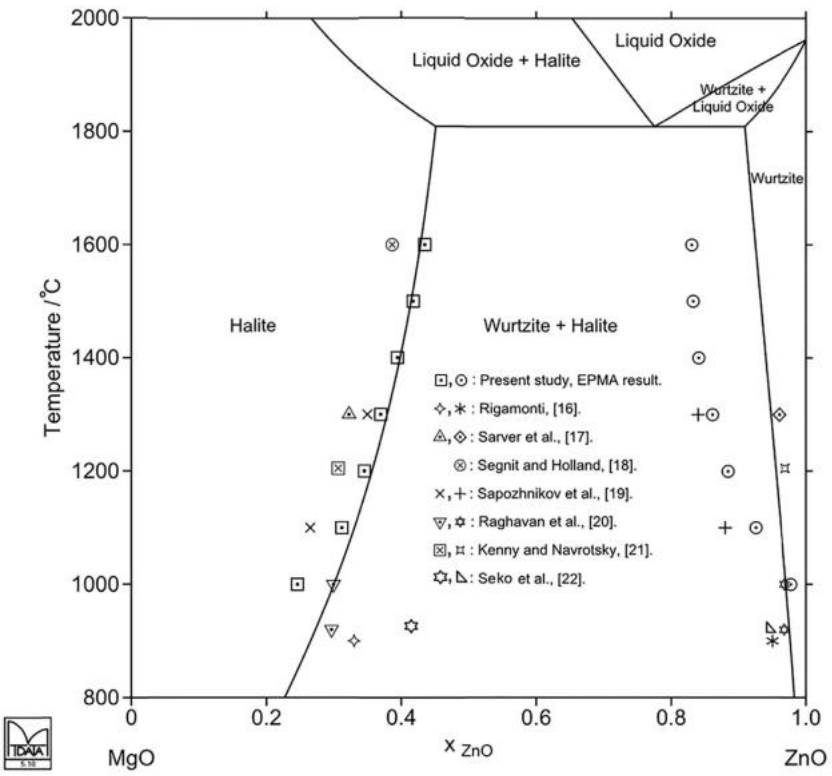

Figure 2.11. Phase diagram of ZnMgO [26]

2.3 Characterization of microcrystals and ZnMgO layers

2.3.1 Raman spectrometry

Raman spectroscopy (Raman) is a non-destructive chemical examination method which provides detailed information about chemical phases and polymorphy, crystallinity and molecular interactions. Raman helps to determine the experimental substances through the vibrations of bound atoms in molecules. It was named after its creator, Chandrasekhara Venkata Raman after he observed this in 1928. Raman scattering is a special type of light scattering that is based upon the interaction of light with the molecular vibrations within a material. In this method, a laser beam with a certain wavelength is focused on the sample. Raman spectroscopy uses laser wavelengths which are not absorbed by the test subject. If the sample molecules and laser light phonons interact with each other, then the molecular vibration gains energy while the scattered light will lose some. The scattered light is therefore shifted compared with the laser light. The Raman shifts have definite wavelengths which respond to the test subjects' chemical structure. Knowing the respective values of Raman peaks in substances, it is possible to determine the compositional and structural nature of samples. That is due to each bond having a unique vibration. Bonds such as C-C, C=C, N-O, etc. [28]–[30]

Using Raman spectrometry, it is possible to analyse many different substances – solids, liquids, gels, gases. A confocal Horiba LabRAM HR800 Micro-Raman system that is used in the study, is presented in Figure 2.12. The device is existing in TalTech. [29]

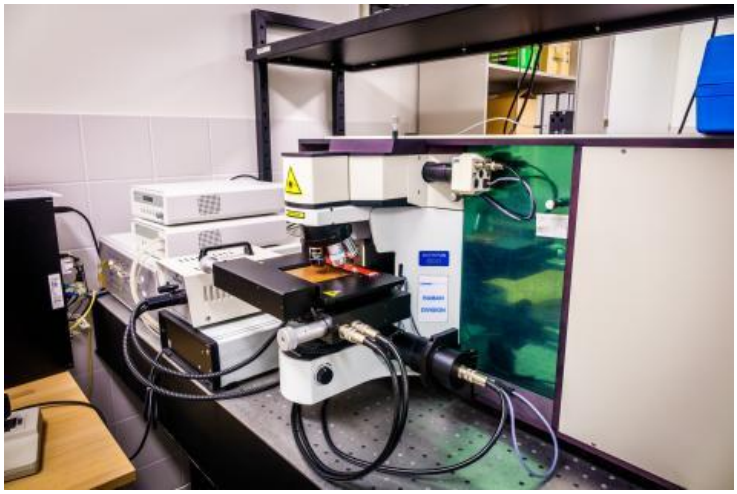

Figure 2.12. Raman spectrometer at TalTech [31]

Each material has its specific Raman spectrum and this way makes it possible to identify what is being tested. Through Raman spectrometry it is possible to get additional information regarding the test substance's chemical structure, phases and impurities. [29]

2.3.2 Scanning electron microscopy (SEM)

Scanning electron microscopy (SEM) is an effective method when analysing objects in a nanometer to micrometer scale. The sample is excited by an electron beam. The atoms inside the substance then interact with the electrons from the beam, creating certain signals. They are usually detected by secondary electrons, but also backscattered electrons, and their analysis provides a SEM image. [32] The morphology of microcrystals in this work was studied by high-resolution scanning electron microscope ZEISS HR SEM ULTRA 55 and shown in Figure 2.13.

Figure 2.13. SEM ZEISS HR SEM ULTRA 55 at TalTech [31]

2.3.3 Sieving

To differentiate microcrystals by their size, sieving was done between size fractions 63-125 µm. This resulted in the following fractions: 63-75, 75-80, 80-90, 90-100, 100-112 and 112-125 µm. The process was done manually. The accuracy of weighing was +/- 0.001 g.

2.4 Solar cell characteristics

2.4.1 Current-Voltage measurements

I-V measurements help to gain understanding of electrical parameters of a PV element. The characteristic curve depicts the relationship between the current flowing through a device and the voltage that is applied across. The data enables to learn more about its efficiency and energy conversion capacity. This also helps in developing a system where it could function near its maximum power point (MPP). [33]–[35]

A scheme of an I-V curve is depicted in Figure 2.14. Open-circuit voltage (V_{OC}) is measured when the device is not connected to a load and the voltage is at its highest while current is at its lowest value. Short-circuit current (I_{SC}) is observed when the solar cell is attached to a load and where it will produce its maximum current. Measuring this it is possible to assess how many amperes the device can handle. MPP is a point where the power value reaches its highest, with values V_{MP} and I_{MP}. [35], [36]

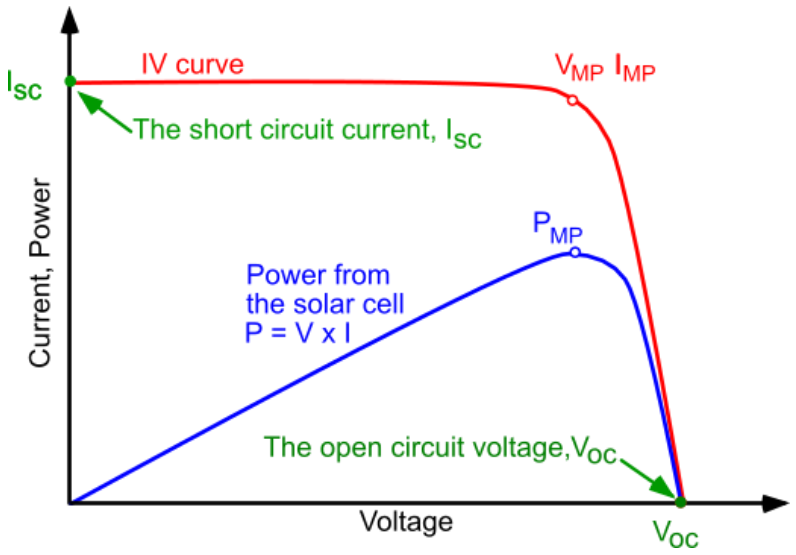

Figure 2.14. I-V curve [37]

In a perfect situation, the relation between current and voltage is linear at a constant temperature. Due to irradiance and temperature fluctuation, solar cells have a non-linear I-V curve. [34], [35]

In Figure 2.15, Keithley 2400 existing in TalTech was used to measure solar cell's parameters such as open-circuit voltage (V_{oc}), short-circuit current density (J_{sc}), fill factor (FF) and efficiency (η). Tests included measurements in both, in dark and under

standard test conditions using light with illumination intensity of 100 mW/cm^2 (AM 1.5). [38]

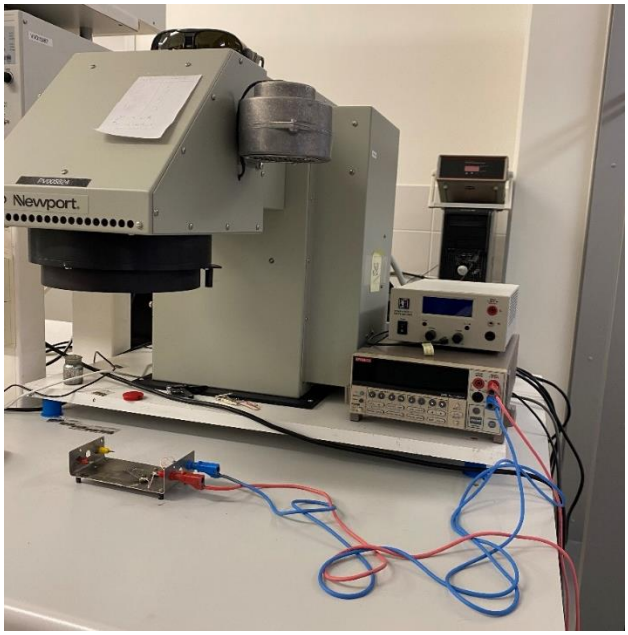

Figure 2.15. I-V measurements were carried out on Keithley 2400 – right. Left: Newport AAA class solar simulator

2.4.2 Quantum efficiency measurements

The quantum efficiency is the technique where we measure the ratio of the number of charge carriers collected by the solar cell to the number of photons of given energy incident on the solar cell. Usually, the quantum efficiency is given as a function of wavelength. Figure 2.16 describes what can be read from the quantum efficiency curve. The brown line shows the ideal values, but in the real world, there are always losses such as reflection, low and high diffusion lengths depending on the wavelength. If all photons of a certain wavelength are absorbed and the resulting minority carriers are collected, then the quantum efficiency at that particular wavelength is unity. The quantum efficiency for photons with energy below the band gap is zero. [39]

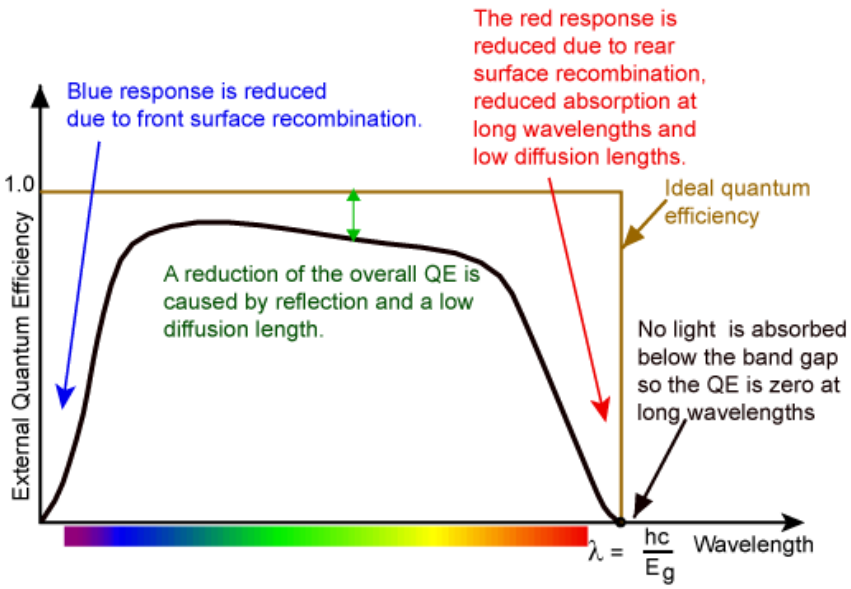

Figure 2.16. Quantum efficiency curve [39]

For external quantum efficiency measurements (EQE) a 100 W calibrated halogen lamp was used as a light source together with a SPM-2 prism monochromator. Monochromatic and modulated (120 Hz) light was focused on the front surface of the solar cell. The generated short circuit current was detected with a DSP Lock-In amplifier (SR 810). Equipment used is presented in Figure 2.17. From the quantum efficiency curves the absorber bandgap energy was also estimated, in order to evaluate is there any effect to the bandgap value by different selenium microcrystals fabrication techniques. [38]

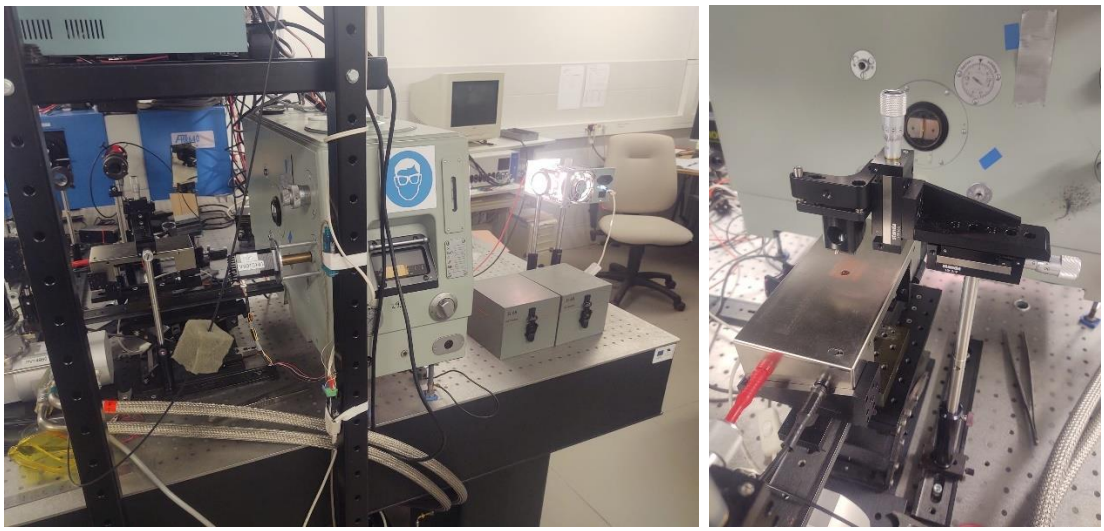

Figure 2.17. Equipment used for EQE measurements at TalTech [31]

3 RESULTS AND DISCUSSION

In this chapter of the study, the results of made experiments are presented. This includes preparation of selenium microcrystals, *n*-type buffer layer ZnMgO deposition and completion of a solar cell. Each of these steps was analysed, using methods such as Raman, SEM, I-V and Quantum efficiency measurements. The discussion will follow.

3.1 Morphology of selenium microcrystals

The initial granules (purity 99,999%) were ground (crashed) in a mortar and sieved through different sieves to get almost unisize pieces of selenium powder. After cooling down from heating to the room temperature, Raman Spectroscopy as well as Scanning Electron Microscopy were used for the characterization of microcrystals'. In the present study, the following technological parameters were changed: heating temperature, cooling rate, environment (vacuum, gas), rate of gas flow in the heating system. In some tests, the peaks of Raman spectra showed fully amorphous grains and sometimes both, amorphous and trigonal grains were found.

In Figure 3.1 SEM images of Se grains of the first heating test are presented. The grains are spherical balls with smooth surfaces. When reaching temperature close to the selenium melting point, microcrystals tend to stick together to form bigger grains. From this it could be concluded that the grains had been at temperature high enough to melt the grains (if selenium melts, it forms a round shape), but the cooling time was too short to enable grains to rearrange.

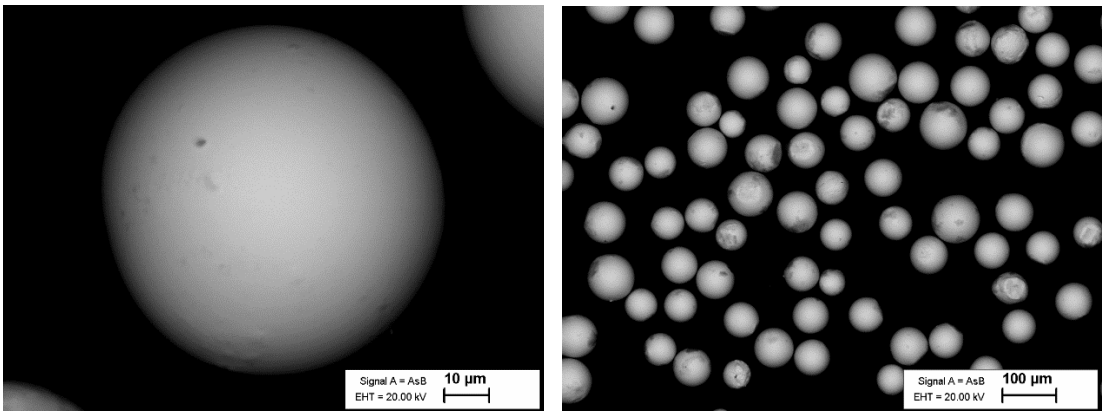

Figure 3.1. SEM images of amorphous selenium grains produced using three-zone furnace method

Learning from the first experiment, the cooling time was prolonged. As mentioned before, cooling time was one of the main parameters when it comes to rearranging. Too long cooling time means prolonged time for this step. As a result, the grain boundaries become defined as seen in Figure 3.2 (cooling time 5 hours).

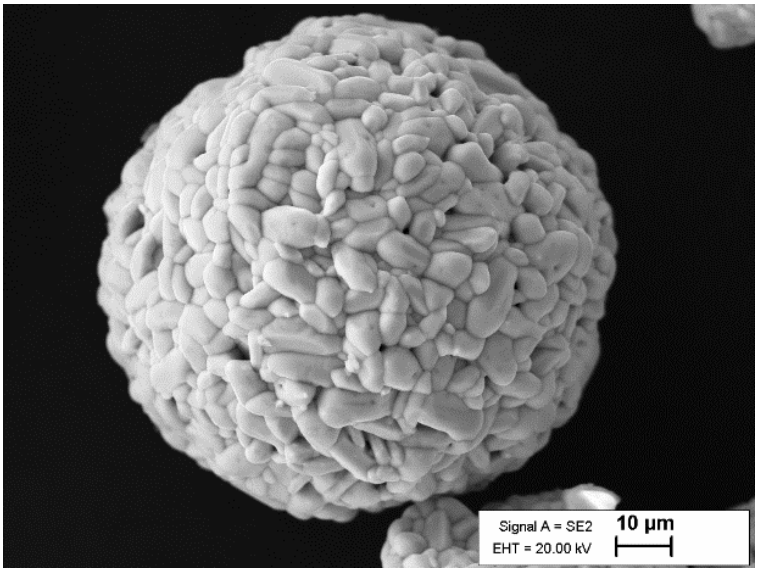

Figure 3.2. Se microcrystal, long cooling time

To achieve a cooling rate between those before mentioned, cooling time was changed again, decreased to 3 hours. Figure 3.3 presents the SEM images of microcrystals prepared in three-zone furnace (Figure. 2.15). Due to nearing the melting temperature, the grains tend to stick together. This is seen on the right in Figure 3.3.

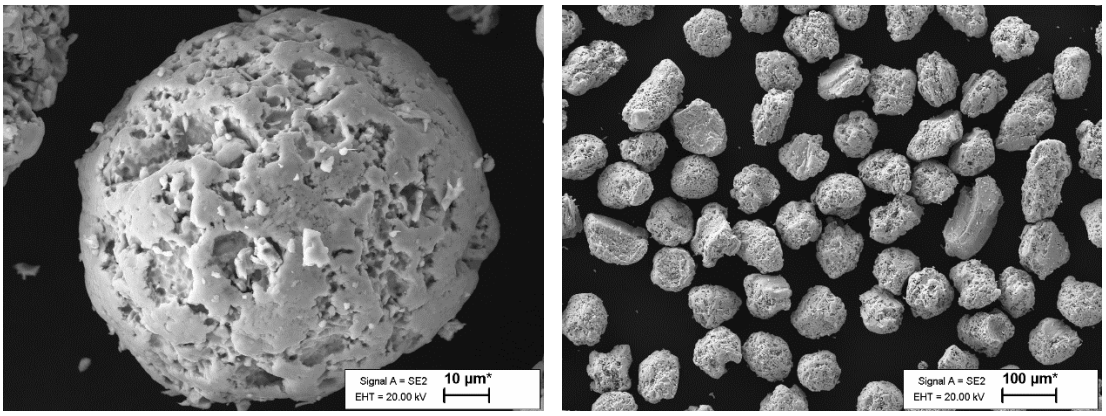

Figure 3.3. SEM images of grains of trigonal selenium, processed in the three-zone furnace

Although the previous experiment showed a promising result, alternative methods were looked at. Muffle furnace was the additional step to decrease transformation time and increase the amount of microcrystals created. The result seen in Figure 3.4 is quite

similar to Figure 3.3 but more definite grain boundaries are seen. Also, the grains tended to stick together more, therefore creating bigger, bundles.

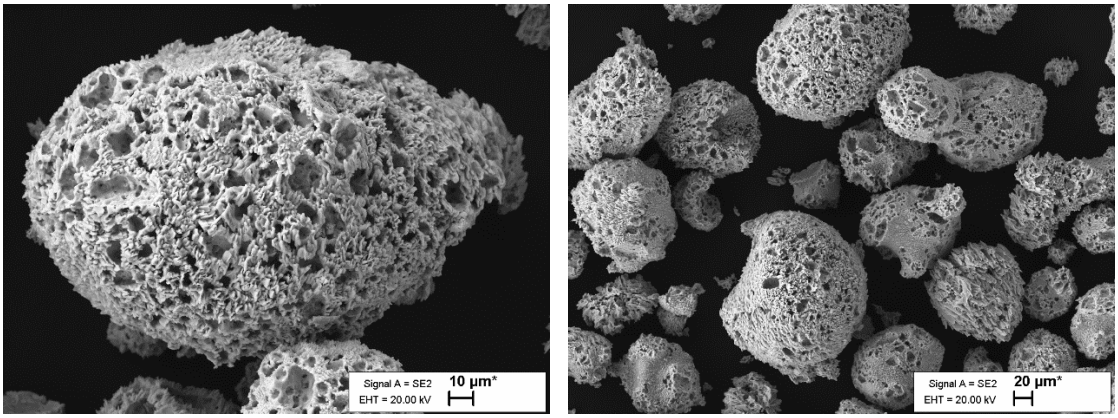

Figure 3.4. SEM images of Se grains recrystallised in the muffle furnace

Raman spectra of Se grains shown in Figures 3.3 and 3.4 were characteristic to the *t-Se*. From this observation, it can be concluded that the grains were recrystallized. But the used arrangement allowed the production of small amounts of selenium grains.

In order to produce bigger amounts of grains, additional crystallisation method was needed. With this in mind, next recrystallization of Se grains was performed in an ampoule by mixing Se particles with solid KI powder. A ratio of 1:2 was chosen. 5g of Se and 10g of KI were weighed and mixed together.

In Figure 3.5 selenium grains heated in ampoule are shown. Microcrystals' appearance is relatively different from the previous experiments. The grains are not of homogenous shape and size, indicating that the grains did not reach melting phase and further temperature increase is needed.

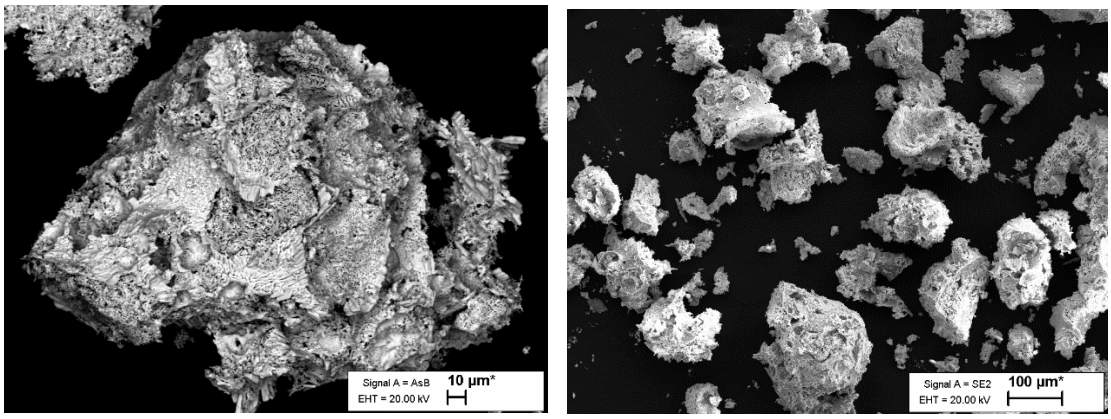

Figure 3.5. SEM images of *t-Se* grains heated in solid KI

3.2 Phase composition of Se

Initial selenium was in the form of big granules with a diameter of about 5 mm. The Raman spectrum of the precursor Se is presented in Figure 3.7. There can be seen Raman peaks that are not sharp and characteristic to the *t-Se*. Characteristic Raman peaks of *t-Se* are doublets at 234 cm^{-1}. [19] It is very probable that the precursor contains some part of amorphous phase. In order Io guarantee that selenium is transformed into crystalline form, the grains need to be heated from room temperature to around their melting temperature which allows the transformation of grains' structure fully to *t-Se.* [19] The gradual slow cooling is required to give enough time for atoms to rearrange. The cooling process is the most important step in the reformation of selenium. Too slow cooling will lead to microcrystals cracking and too fast cooling could prevent them from rearranging and the material will stay partly in amorphous phase [4].

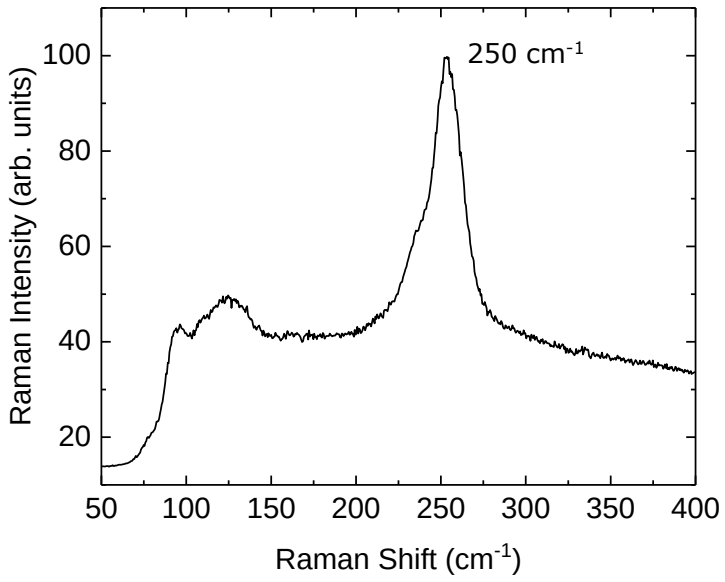

Figure 3.6. Raman spectrum of Se used as precursor in recrystallization experiments

The ground and sieved Se pieces (fraction 63-75 μm) were distributed onto a graphitized plate and the plate with Se pieces was moved into the central zone of the furnace. After closing the ends of tube, the tube was evacuated by vacuum pump and filled with nitrogen up to 780 Torr. When the pressure stayed constant, the heating program was started. In the first experiment, Se grains were heated to 230 °C, it means about 10 degrees above the melting temperature of selenium and then cooled with the rate of 0.25 °C/min for an hour. Melting temperature of precursor Se was determined

experimentally in our lab by Dr. K. Timmo and the experimental thermal heating curve is given in Figure 2.2.

The Raman spectrum of heated Se is presented in Figure 3.7. Double peaks positioning at 234 cm^{-1} and 239 cm^{-1} are characteristic to the *t-Se* phase.

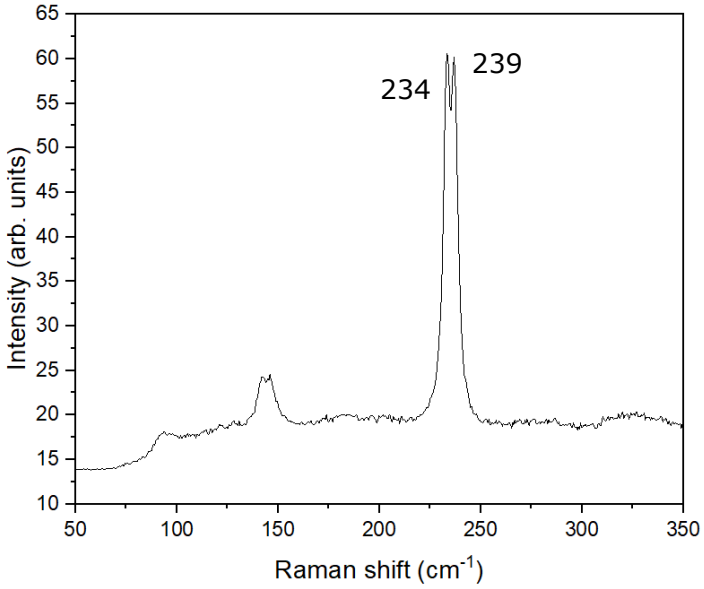

Figure 3.7. Raman spectrum of selenium with characteristic doublets of *t-Se*

Since there were multiple methods how the selenium microcrystals were transformed, each presented a different result. In Figure 3.8 are brought out sample results for each approach. Images a) and b) belong to three-zone furnace Se microcrystals, a) being still in an amorphous phase, matching the Raman spectrum of the precursor Se and b) in a tetragonal form. The difference between two first images is the cooling time. Image a) in Figure is measured after fast cooling and b) from slow cooling. c) is measured from the experiments carried out in a muffle furnace. Both, b) and c) present characteristic doublets of *t-Se*m shown also in Figure 3.7 and d) microcrystals synthesized in KI flux, show a *a-Se* phase.

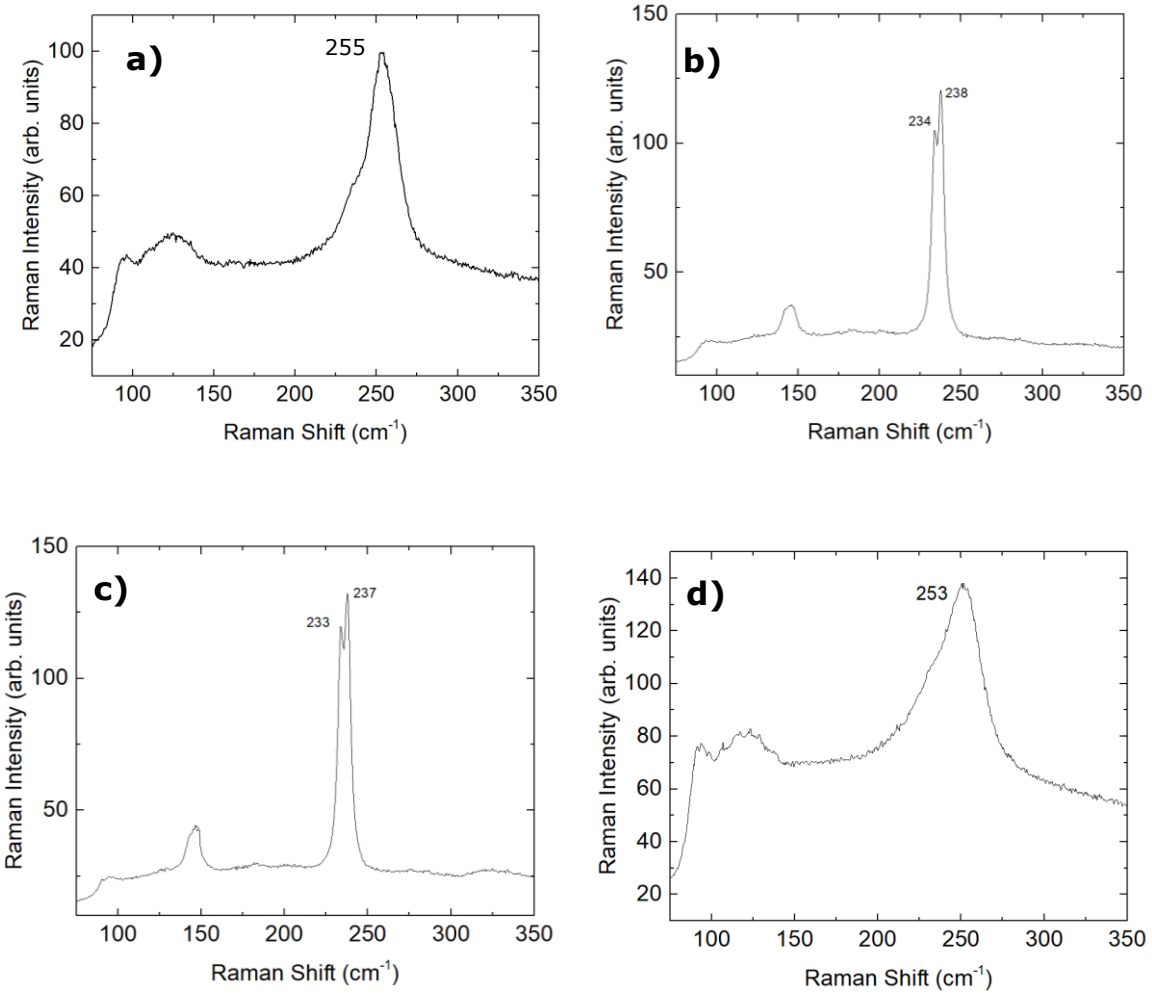

Figure 3.8. Raman spectra showing phase compositions of each method: a) Three-zone furnace, fast cooling; b) Three-zone furnace, slow cooling; c) Muffle furnace; d) Heating in sealed ampoule in KI.

3.3 ZnMgO layer deposition

3.3.1 Chemical composition of solution for ZnMgO deposition

Before the deposition of ZnMgO layer onto a membrane with selenium grains, several depositions onto ITO and FTO conductive glasses were performed in order to find out proper deposition conditions. The solution for ZnMgO layer deposition was made from the next components: liquid NH_4OH (3 M) and $ZnSO_4 \cdot 7H_2O$, $C_6H_8O_7$ (citric acid), $MgSO_4 \cdot 7H_2O$ in powder form.

Before starting the experiment, amounts of substances were determined for making deposition solution. 100 ml of solution was thought to be enough for deposition needed. Different amounts and mixing order were tested to achieve the most uniform layer. Tested were the ratios of magnesium and zinc. Also, volume of the solution was reduced after the first deposition, since a smaller amount was enough to cover the vessel put inside the chemical bath. Table 3.1 shows the chemical composition of solution for the third experiment done (regime 3) where the result was an even layer of ZnMgO, without holes and haing suitable thickness.

Table 3.1. Chemicals added for making 100 ml solution in regime 3

Chemical	Quantity	Concentration, M
$ZnSO_4 \cdot 7H_2O$	0.9202 g	0.5
NH_4OH	4.2 ml	3
$C_6H_8O_7$	0.015 g	0.1
$MgSO_4 \cdot 7H_2O$	0.232 g	0.1

3.3.2 Deposition process

Before deposition onto conductive glasses the glass substrates were cleaned to degrease with hot H_2SO_4 for 30 minutes. For ITO conductive layer surface activation, the degreased glass substrates were inserted for few seconds into a mixture of $HCl+HNO_3+H_2O$ in ratio of 47.5 ml+5 ml+47.5 ml as suggested by producer of ITO glasses. Selenium membranes were cleaned before buffer layer deposition in 10 % KCN solution.

First, the adding order of the chemicals into solution was tested. In the first experiment the components were added in the following order: citric acid was dissolved in water, then NH_4OH, zinc and magnesium sulphates were added. The deposition resulted in layers that were thin and uneven. To improve the layer quality, a new recipe was tested. The volume of solution was decreased to 80 ml. First citric acid was dissolved and NH_4OH was diluted with water and left for 15 minutes for complex formation. While the solution was forming, $ZnSO_4 \cdot 7H_2O$ and $MgSO_4 \cdot 7H_2O$ were weighed and both dissolved in 20 ml water separately. When 15 minutes had passed, the first solution (ammonia + citric acid) was mixed with $ZnSO_4$ solution and then with the $MgSO_4 \cdot$solution. $MgSO_4 \cdot$solution was added last, because, according to the ZnO MgO phase diagram, the thermodynamic

solubility limit of ZnO in MgO is relatively higher than MgO in ZnO. [27] The scheme for making this solution is shown in Figure 3.7.

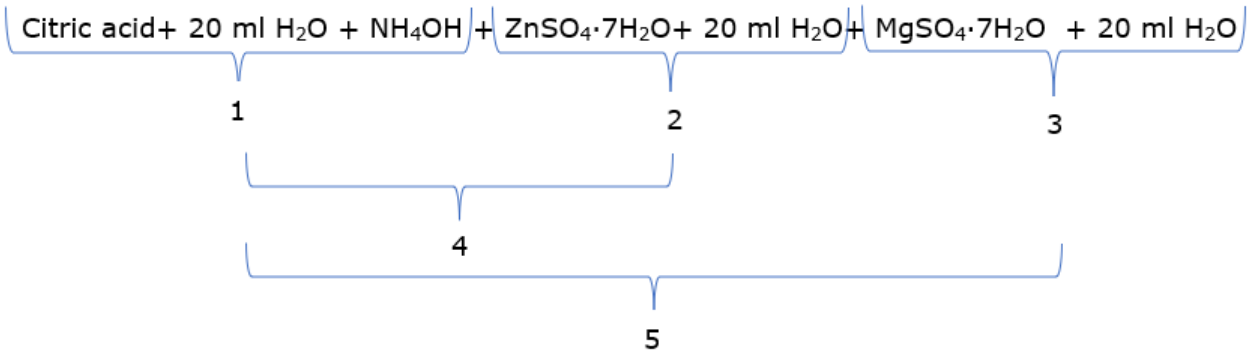

Figure 3.9. Schematic of mixing order of ZnMgO in regime 5

When the solution was ready, it was the time to start the deposition process. Water heating bath had already been heated to 80 °C. The cleaned and activated glass substrates were carefully placed into a special sample holder. The deposition solution was poured into a bigger glass bottle with a magnetic mixing bar and placed into the preheated water bath. Then the sample holder with glass samples was inserted into solution and the deposition process started. The samples were taken out of solution after different time periods to find out the best deposition time (ZmMgO layer thickness)

In Table 3.2, there are shown different parameters that were tested to ensure the best coverability and quality of layers. In addition to etching, surface activation and plasma treatments were experimented. Different deposition times helped to gain understanding what would be the optimal time. Regime 5 was the first time ZnMgO was deposited onto a selenium microcrystal layer.

Table 3.2. Parameters for each deposition regime

	Etching	Surface activation	Plasma treatment	Ultrasonic bath (US)	Deposition times, min	On which surface
Regime 1	H_2SO_4	No	No	No	20	ITO FTO

Regime 2	H_2SO_4	No	No	No Yes Yes	30 30+10 US 15+10 US+15	ITOFTO
Regime 3	H_2SO_4 warm	No	No	No	10 20 30	ITO FTO
Regime 4	No H_2SO_4	$HCl+HNO_3$ No	Yes Yes	No	15	ITO FTO
Regime 5	No No H_2SO_4	No	Yes Yes No	No	15	Se ITO FTO

After the experiments, a graph was made describing how thickness of ZnMgO layer depends on time. This is brought out in Figure 3.10. Thicknesses taken are averages of measured layers. The growth could be described as linear as the thickness increases with time.

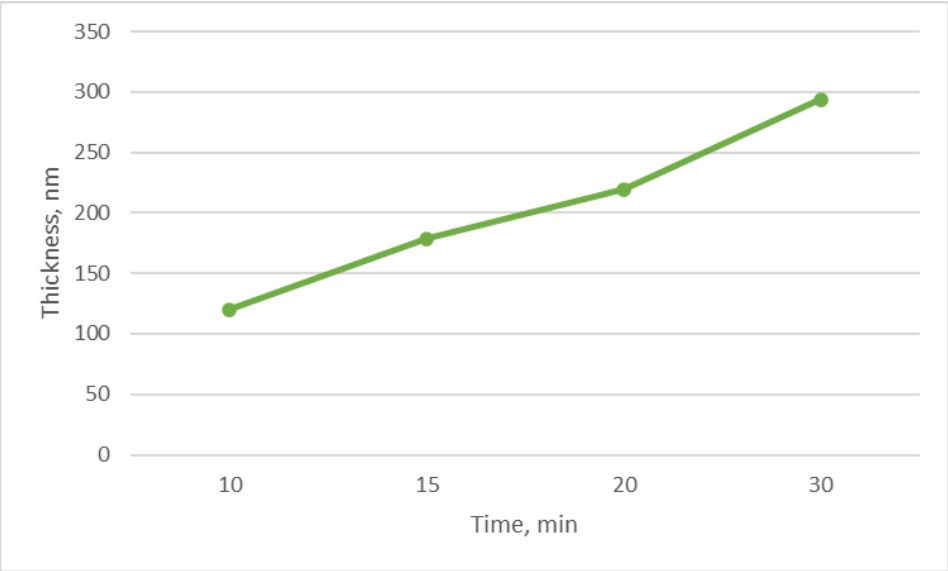

Figure 3.10. Time dependence of ZnMgO layer thickness

As a result, 15 minutes was chosen as deposition time. Tests showed that this allowed growth of a pinhole-free continuous homogeneous layer.

3.3.3 Deposition of ZnMgO on ITO and FTO

Experiments with ZnMgO deposition onto ITO and FTO glasses were made with the aim to analyse the ZnMgO layers' thickness and coverage quality and find out the proper conditions for deposition before depositing it onto a Se membrane.

In Figure 3.11 the ZnMgO layers deposited (Regime 4) onto ITO are seen. Before deposition, ITO surface activation in $HCl+HNO_3$ mixture was done. As can be seen, the resultant ZnMgO layer is even with thickness of around 30 nm. On the left, the layer is uneven, with some parts showing a thicker layer deposited there. Right image shows, in contrast a very even layer of ZnMgO.

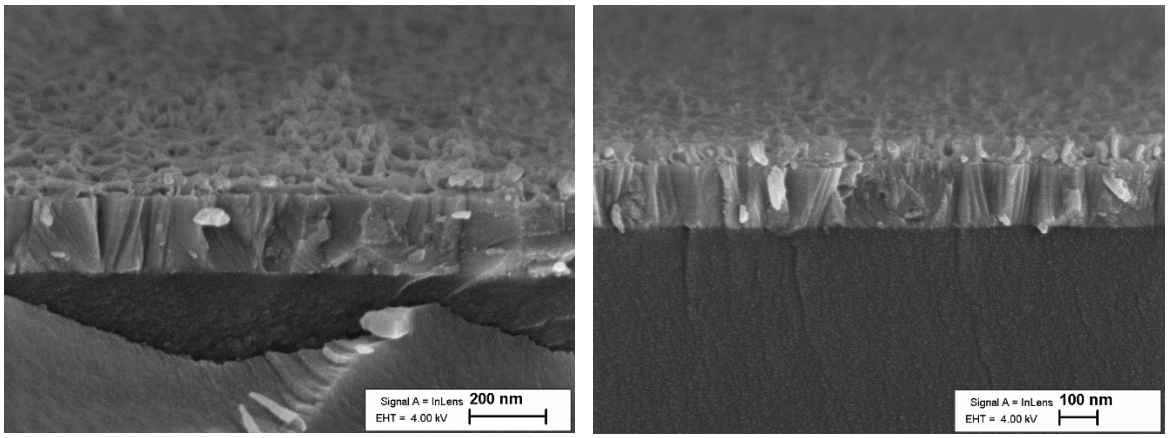

Figure 3.11. Cross-sectional SEM images of ZnMgO layers on ITO

Different types of surfaces were tested to see, how they respond to the deposition process. In addition to ITO, results from deposition on FTO glass are shown in Figure 3.12. On the left image, the layer has big colloids on top. This means that the layer does not have uniform thickness, but some places are very thick while the others the opposite.

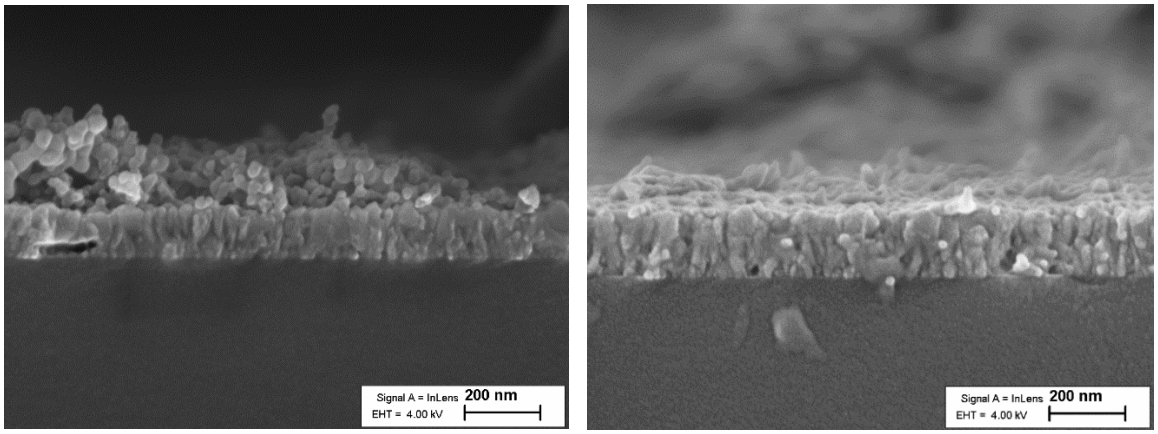

Figure 3.12. Cross-sectional SEM images of ZnMgO layers on FTO

3.3.4 Deposition of ZnMgO on Se membrane

After preliminary ZnMgO deposition experiments onto ITO and FTO glasses, deposition onto Se membrane was done.

The cross-sectional SEM image of a ZnMgO layer deposited onto Se membrane, that was fabricated from the grains that were grown in three-zone furnace, is shown in Figure 3.13. This ZnMgO layer was deposited by Regime 5, deposition time was 15 minutes. Left image shows an individual grain with continuous and even layer of ZnMgO on top of selenium. Right image of Figure 3.13 displays a cross-sectional close-up of the buffer

layer. It could be seen that the layer of ZnMgO is thicker in some areas, but overall coverage seems to be homogeneous.

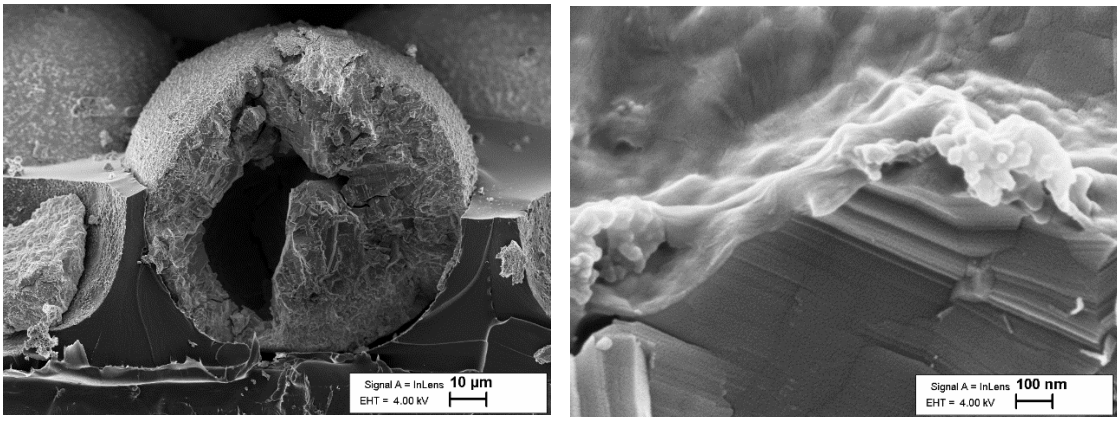

Figure 3.13. Cross-sectional SEM images of ZnMgO layer on selenium

3.4 Solar cell

In order to complete the ZnMgO/Se solar cell, first a layer of i:ZnO and then ZnO:Al were deposited on top of the structure. What was done at this point, is that there was a selenium membrane with ZnMgO buffer layer i:ZnO and ZnO:Al.

A silver nanorods' diluted paste with dilution 1:1 was added onto membrane surface to improve the planar carrier collection A droplet of solution was added to the edge, distributed evenly over the membrane and left to dry for 30 minutes. In Figure 3.14, a Se membrane is shown. Due to fabrication of small amounts of Se at a time, the ready membranes were miniature.

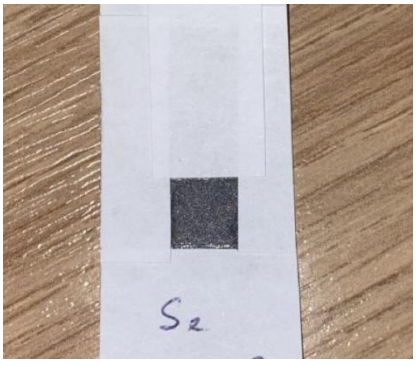

Figure 3.14. Se membrane

I-V measurements were done for multiple contacts on a selenium MGL solar cells, but presented is the data for the highest achieved efficiency in this study, in Figure 3.15. It was measured on the third made solar cell with gold contacts.

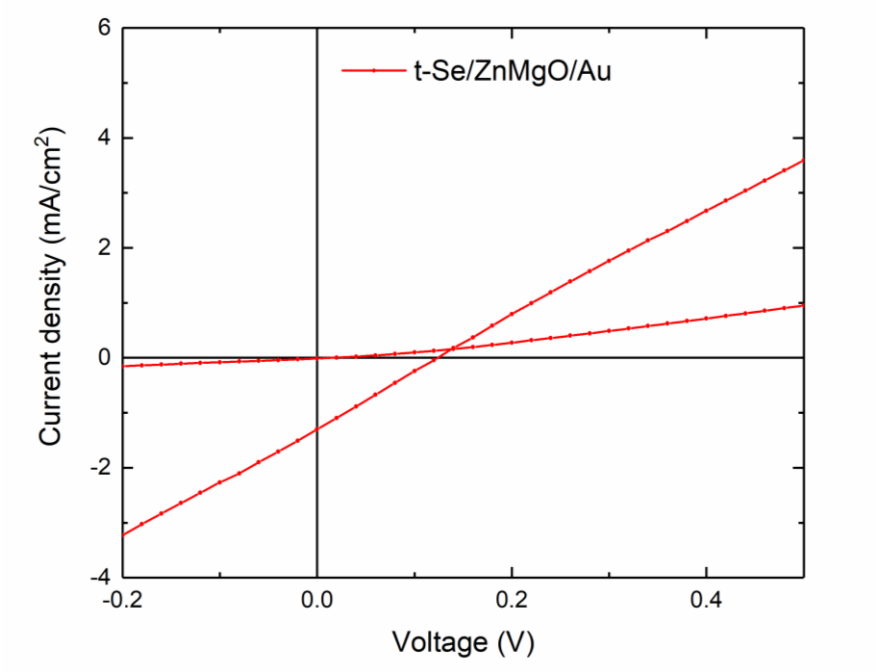

Figure 3.15. I-V curve measurements of SeKL3

The reason why the I-V curve graph looked out of the ordinary could be because the short-circuit is leaking. That means that there are faults inside the layers. It could be concluded that even though SEM images showed a homogenous pinhole free continuous buffer layer, the process could be improved.

Table 3.3 presents the parameters of highest efficiency solar cell achieved in this study – 0.0402%. Tested area is the size of applied gold contact - 0.045 cm^2.

Table 3.3. Parameters of SeKL3 solar cell

V_{oc}	123.7 mV
I_{sc}	-0.005858 mA
FF	25%

Efficiency	0.0402%

Quantum efficiency measurements were done to evaluate the optical and electronic losses in the solar cell and also estimate the band gap of selenium micrograin solar cell.

Solar cell called as SeKL3 was used to measure the characteristics and three different contacts were measured. Quantum efficiency measurements were focused on two different sides: 452 nm and maximum value to observe if the difference was more due to buffer or absorber layer, to observe the differences of each contact. In Figure 3.16, the QE is normalized at 452 nm. From the figure, it could be seen that one contact (blue line) shows weaker signal than the others. This could be due to selenium microcrystals not having an uniform shape or were in *a-Se* phase.

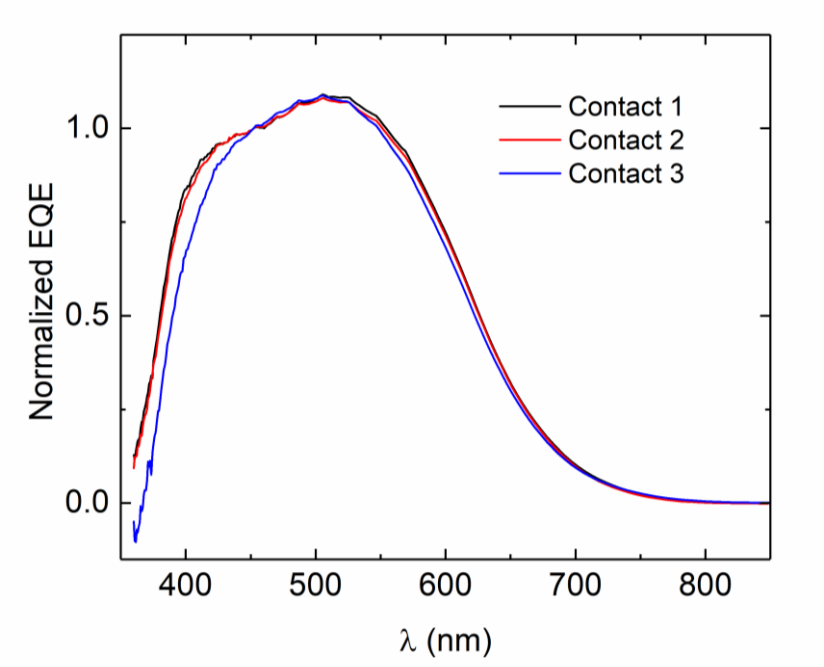

Figure 3.16. Normalized quantum efficiency at 452 nm

In Figure 3.17, the quantum efficiency graph is normalized at maximum value. In contrast to previous figure, the same contact (blue line) indicates a different value than other when normalized at maximum value. This could indicate that the ZnMgO layer had better pinhole-free homogenous coverage at that contact.

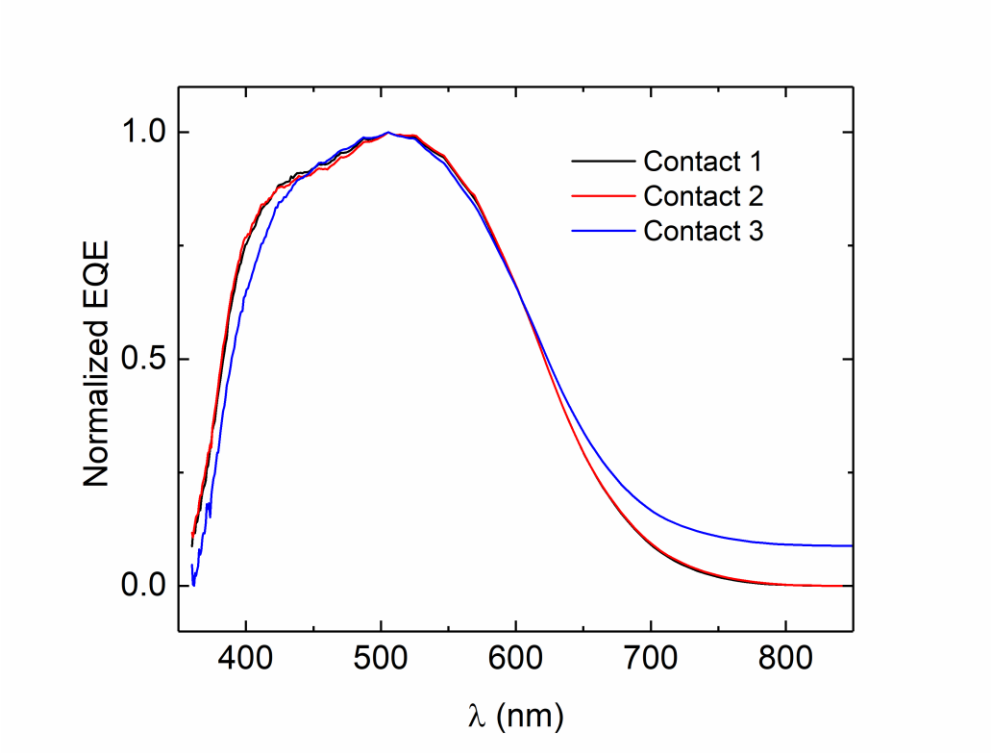

Figure 3.17. Normalized quantum efficiency at max value

As seen in Figure 3.18, the bandgap value of Se, determined via EQE measurements was 1.83 eV, matching well with the literature sources.

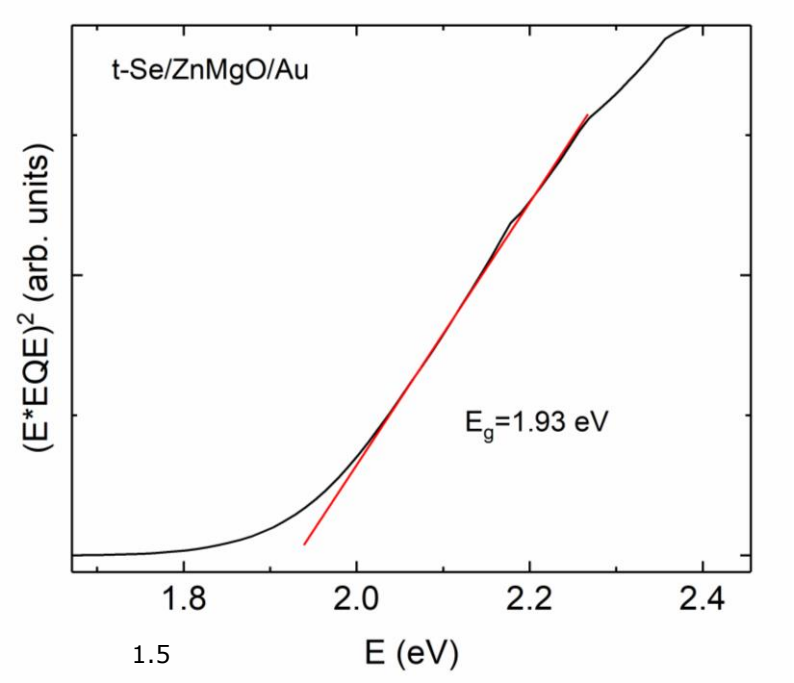

Figure 3.18. Se bandgap determination from external quantum efficiency dependence of SeKL3 solar cell

Selenium is a semiconductor that has a direct bandgap. The effective band gap energy E_g can be calculated using an approximation from the low energy side of the EQE curve, that meaning, near the band gap energy $E \approx E_g$. [40] Equation 3.1 presents the conclusion proposed by Klenk and Shock:

$$EQE \approx K \propto L_{eff} \approx A(E\text{-}E_g)^{1/2}/E \tag{3.1}$$

In this equation, A consists of all energy independent parameters, $L_{eff} = w + L_d$ is the effective diffusion length of minority carriers, where L_d is their diffusion length in the absorber material, w is the width of the depletion region, and α is the absorption coefficient of the absorber material. The constant K is unity in absolute measurements. Plotting the $(EQE*E)^2$ vs E graph, it is possible to detect two linear parts and from it the projecting the band gap energy. [40]

SUMMARY

Within this thesis, the development of a selenium monograin layer solar cell was studied and described. For *p*-type absorber layer, Se microcrystals were prepared using three different methods: three-zone furnace, muffle furnace and in solid KI.

For *n*-type layer, ZnMgO was deposited by CBD method. It was first tested on conductive glasses and when the process was reinforced, on selenium membrane. Both processes were characterized and analysed by Raman Spectrometry and Scanning Electron Microscopy.

After fabrication of *p*- and *n*-type layers, a solar cell was prepared. The characteristics of a PV element were tested by using I-V and Quantum efficiency measurements.

- The process of selenium preparation showed that rather than monograins, microcrystals were formed. The scattered grains tended to stick together to form big non-uniform pieces. That could be due to uneven distribution of selenium on a heating plate. Due to size of the plate as well as the furnaces, it was possible to produce small amounts of microcrystals at a time. This led to preparation of minor size MGL membranes.

- The target in depositing *n*-type buffer layer was to achieve pinhole-free homogenous continuous surface. The mixing order of deposition solution components was tested and modified to achieve the best resultant buffer layer. SEM images showed that the goal was reached, but analysing the results of solar cell testing, this process could be further improved.

- Phase composition of selenium microcrystals was determined by using Raman analysis. This data provided info regarding the phases of the microcrystals before and after heat treatment and allowed to ensure fabrication of *t-Se*. SEM images were taken of both, selenium and ZnMgO layer for examination. For microcrystals this provided knowledge regarding the shape and grain boundaries. For ZnMgO buffer layer, images were used to analyse the thickness, appearance and coverage.

- The highest achieved efficiency of Se monograin layer solar cell within this study was 0.0402%.

Conclusions and possible future improvements that could be taken from this study:

- It was possible to transform the phase of selenium microcrystals from *a-Se* to *t-Se*. However, due to melting together and creating bundles, the preparation process for producing monograin selenium could be perfected.

During this thesis the study about suitability of selenium for monograin layer solar sell absorber was carried out. An immense number of experiments were done. This could be the basis to continue researching this field.

KOKKUVÕTE

Käesoleva lõputöö raames võeti vaatluse alla võimalused seleen-monoterakiht päikeseelemendi praktiliseks valmistamiseks. *P*-tüüpi absorberkihi jaoks kasutati Se mikrokristalle, mida sünteesiti kolmel erineval viisil: kuumutamisel kolme tsooniga toruahjus, kamberahjus ja kinnises ampullis segatuna tahke KI pulbriga.

N-tüüpi juhtivusega ZnMgO kihi sadestamiseks keemilise vanni meetodil uuriti lahusekomponentide lisamise järjestuse ja sadestusaja mõju kihi paksusele, kattuvusele ja pidevusele. Nimetatud kihi sadestuse uurimiseks kasutati juhtivaid klaasaluseid. Katsetulemuste põhjal valiti režiim ZnMgO puhverkihi sadestamiseks Se monoterakiht-membraanidele. Sadestatud kihtide uurimiseks kasutati Raman Spektromeetriat ja Skanneerivat Elektronmikroskoopiat (SEM).

Peale *p*- ja *n*-tüüpi kihtide tehnoloogia testimist valmistati päikeseelement. PV elemendi karakteristikuid uuriti, kasutades I-V ning kvantefektiivsuse mõõtmisi.

- Seleenitükikeste kuumutamise tulemusena tekkisid pigem mikrokristallide kogumikud, mitte monoterad. Plaadile laialipuistatud terad kippusid kokku sulama, moodustades suuri ebaühtlasi kogumikke. Selle võis põhjustada ebaühtlane seleeni jaotus alusel. Plaadi ja ahjude suuruse tõttu oli võimalik korraga toota vaid väga väike kogus mikrokristalle. Selle tõttu olid ka valminud MGL membraanid pisikesed.

- *N*-tüüpi juhtivusega ZnMgO valmistamise eesmärk oli sadestada aukude-vaba homogeenne pidev kiht. Protsessi katsetati ja vajadusel muudeti, et saavutada parim tulemus. SEM piltidelt on näha, et seatud ülesanne täideti, kuid päikeseelemendi testide kaudu tuli tõdeda, et seda protsessi tuleb parendada.

- Seleeni mikrokristallide faasiline koostis määratleti, kasutades Raman Spektromeetriat. Teoreetilise tausta uurimisel omandatud info faaside kohta ning testimine enne ja pärast termilist töötlemist võimaldas kinnitada *t-Se* formeerumist. SEM pildid tehti analüüsi eesmärgil nii seleenist kui ka ZnMgO-st. Mikrokristallide puhul andis see infot kuju ja terapiiride kohta. ZnMgO puhverkihi piltide abil oli võimalik analüüside kihi paksust, väljanägemist ja katvust.

- Kõrgeim saavutatud Se- monotrakiht päikeseelemendi efektiivsus selles töös oli 0.0402%

Järeldused ja võimalikud tuleviku uurimissuunad, mis sellest tööst võtta:

- Edukaks saab lugeda seleeni mikrokristallide faasilise koostise muutmist amorfsest tetragonaalsesse faasi. Kuid kokku sulamise ja pundarte moodustamise tõttu tuleks prepareerimise protsessi täiustada, et toota seleeni monoterasid.

Lõputöö kestel vaadeldi, kui jätkusuutlik on seleeni kasutamine monoterakihi jaoks. Selleks viidi läbi ulatuslik arv eksperimente ja testimisi. See töö võiks olla põhjaks tuleviku uurimuste baasiks.

LIST OF REFERENCES

[1] L. El Chaar, L. A. lamont, and N. El Zein, 'Review of photovoltaic technologies', *Renewable and Sustainable Energy Reviews*, vol. 15, no. 5, pp. 2165–2175, Jun. 2011, doi: 10.1016/j.rser.2011.01.004.

[2] European Commission. Directorate-General for Energy, *Energy : roadmap 2050*. LU: Publications Office, 2012. Accessed: Apr. 26, 2022. [Online]. Available: https://data.europa.eu/doi/10.2833/10759

[3] P. Hersch, K. Zweibel, and S. E. R. Institute, 'Basic Photovoltaic Principles and Methods', p. 71.

[4] I. Hadar, T.-B. Song, W. Ke, and M. G. Kanatzidis, 'Modern Processing and Insights on Selenium Solar Cells: The World's First Photovoltaic Device', *Advanced Energy Materials*, vol. 9, no. 16, p. 1802766, 2019.

[5] 'Solar Radiation Basics', *Energy.gov*. https://www.energy.gov/eere/solar/solar-radiation-basics (accessed Apr. 13, 2022).

[6] 'A review of photovoltaic systems_ Design, operation and maintenance | Elsevier Enhanced Reader'. https://reader.elsevier.com/reader/sd/pii/S0038092X19305912?token=7E2ED6913D9BE239584E0442B6F5CAE332D5B0851EFF1EB0A792A884EC2B895AB50C526369C397340277401084AF13B2&originRegion=eu-west-1&originCreation=20220309100522 (accessed Mar. 09, 2022).

[7] 'Global Renewable Energy Market Report and Forecast 2022-2027'. https://www.expertmarketresearch.com/reports/renewable-energy-market (accessed May 03, 2022).

[8] 'Band gap - Energy Education'. https://energyeducation.ca/encyclopedia/Band_gap (accessed Mar. 09, 2022).

[9] 'Diode operation - Energy Education'. https://energyeducation.ca/encyclopedia/Diode_operation (accessed Mar. 08, 2022).

[10] admin, 'pn Junction Diode and Its Working Principle', *Electrical Concepts*, Oct. 09, 2018. https://electricalbaba.com/pn-junction-diode/ (accessed Mar. 15, 2022).

[11] D. Berney Needleman, 'Optical design guidelines for spectral splitting photovoltaic systems : a sensitivity analysis approach', Dec. 2014.

[12] 'Formation of a PN-Junction | PVEducation'. https://www.pveducation.org/pvcdrom/pn-junctions/formation-of-a-pn-junction (accessed May 03, 2022).

[13] S. Sharma, K. K. Jain, and A. Sharma, 'Solar Cells: In Research and Applications—A Review', *Materials Sciences and Applications*, vol. 06, no. 12, Art. no. 12, 2015, doi: 10.4236/msa.2015.612113.

[14] A. Nande, S. Raut, and S. J. Dhoble, 'Chapter 9 - Perovskite solar cells', in *Energy Materials*, S. J. Dhoble, N. T. Kalyani, B. Vengadaesvaran, and A. K. Arof, Eds. Elsevier, 2021, pp. 249–281. doi: https://doi.org/10.1016/B978-0-12-823710-6.00002-9.

[15] 'Third-generation photovoltaic cell', *Wikipedia*. Apr. 25, 2021. Accessed: May 17, 2022. [Online]. Available: https://en.wikipedia.org/w/index.php?title=Third-generation_photovoltaic_cell&oldid=1019882455

[16] T. K. Todorov *et al.*, 'Ultrathin high band gap solar cells with improved efficiencies from the world's oldest photovoltaic material', *Nat Commun*, vol. 8, no. 1, p. 682, Dec. 2017.

[17] Y. N. Sudhakar, M. Selvakumar, and D. Krishna Bhat, *Biopolymer Electrolytes. Fundamtentals and Applications in Energy Storage*. Elsevier, 2018.

[18] A. Kunioka and T. Nakada, 'High-Efficiency Selenium Photovoltaic Solar Cells', *Jpn. J. Appl. Phys.*, vol. 21, no. S2, p. 73, Jan. 1982, doi: 10.7567/JJAPS.21S2.73.

[19] 'Raman scattering study on structural and dynamical features of noncrystalline selenium: The Journal of Chemical Physics: Vol 121, No 10'. https://aip.scitation.org/doi/abs/10.1063/1.1780151?casa_token=yivNpftuIHEAAAAA:Jo7ssRCOPZ1mM6npu8iSNu5KMG925ITXMmTyTefrzp1u9-w6-jr6i0xQuUP4sEZ6yOaQaja1aWFA (accessed Apr. 08, 2022).

[20] Materialscientist, *English: Structure of trigonal selenium*. 2009. Accessed: Mar. 22, 2022. [Online]. Available: https://commons.wikimedia.org/wiki/File:Selenium_trigonal.jpg

[21] E. Mellikov *et al.*, 'Monograin materials for solar cells', *Solar Energy Materials and Solar Cells*, vol. 93, no. 1, pp. 65–68, Jan. 2009, doi: 10.1016/j.solmat.2008.04.018.

[22] M. Altosaar *et al.*, 'Monograin layer solar cells', *Thin Solid Films*, vol. 431–432, pp. 466–469, May 2003, doi: 10.1016/S0040-6090(03)00167-6.

[23] E. Mellikov, J. Hiie, and M. Altosaar, 'Powder materials and technologies for solar cells', *International Journal of Materials & Product Technology - INT J MATER PROD TECHNOL*, vol. 28, Jan. 2007, doi: 10.1504/IJMPT.2007.013082.

[24] S. Li, M. Altosaar, and M. Pilvet, 'Optimization of Buffer Layer for Copper-Zinc-Tin-Sulfide-based Solar Cells', Jun. 2016, Accessed: May 10, 2022. [Online]. Available: https://digikogu.taltech.ee/et/Item/c769b614-4c26-4504-a361-de9385f0ef91

[25] 'Monograin Layer Solar Cell Technology for Space Application', *issuu*. https://issuu.com/eas-estonia/docs/estonian_space_technologies_phone_book_2020/s/11869700 (accessed May 03, 2022).

[26] L. Xia, Z. Liu, and P. Taskinen, 'Solubility study of the halite and wurtzite solid solutions in the MgO-ZnO system within temperature range from 1000 to 1600 °C', *Journal of Alloys and Compounds*, vol. 687, pp. 827–832, 2016, doi: https://doi.org/10.1016/j.jallcom.2016.06.191.

[27] J. L. Morrison *et al.*, 'Optical properties of ZnO and MgZnO nanocrystals below and at the phase separation range', *Journal of Applied Physics*, vol. 104, no. 12, p. 123519, Dec. 2008, doi: 10.1063/1.3043609.

[28] M. Baudelet, '15.1.3 Raman Spectroscopy', in *Laser Spectroscopy for Sensing - Fundamentals, Techniques and Applications*, Elsevier, pp. 466–470. [Online]. Available: https://app.knovel.com/hotlink/pdf/id:kt00U8D7S1/laser-spectroscopy-sensing/applicatio-raman-spectroscopy

[29] 'What is Raman Spectroscopy? - HORIBA'. https://www.horiba.com/en_en/raman-imaging-and-spectroscopy/ (accessed Nov. 23, 2020).

[30] R. Kaupmees, J. Krustok, and M. Grossberg, 'Growth and Optical Properties of Two-Dimensional Transition Metal Dichalcogenides', Jun. 2021, Accessed: Apr. 01,

2022. [Online]. Available: https://digikogu.taltech.ee/et/Item/72b400aa-c5da-4db6-8cb0-acce54153e2a

[31] 'Päikeseenergeetika materjalide teaduslabor | TalTech'. https://taltech.ee/materjali-ja-keskkonnatehnoloogia-instituut/paikeseenergeetika-materjalide-labor (accessed May 08, 2022).

[32] A. Mohammed and A. Abdullah, 'SCANNING ELECTRON MICROSCOPY (SEM): A REVIEW', p. 9.

[33] E. D. Aranda, J. A. Gomez Galan, M. S. de Cardona, and J. M. Andujar Marquez, 'Measuring the I-V curve of PV generators', *IEEE Industrial Electronics Magazine*, vol. 3, no. 3, pp. 4–14, Sep. 2009, doi: 10.1109/MIE.2009.933882.

[34] 'I-V Characteristic Curves or Current-Voltage Curves', *Basic Electronics Tutorials*, Oct. 17, 2013. https://www.electronics-tutorials.ws/blog/i-v-characteristic-curves.html (accessed May 09, 2022).

[35] 'Solar Cell I-V Characteristic and the Solar Cell I-V Curve', *Alternative Energy Tutorials*. https://www.alternative-energy-tutorials.com/photovoltaics/solar-cell-i-v-characteristic.html (accessed May 09, 2022).

[36] A. Rathore, 'Difference Between Nominal Voltage, Voc, Vmp, Isc And Imp', *Electronics For You*, Nov. 20, 2020. https://www.electronicsforu.com/market-verticals/solar/difference-nominal-voltage-voc-vmp-isc-imp-solar-panels (accessed May 09, 2022).

[37] Lindholm, J. G. Fossum, and E. L. Burgess, 'Application of the superposition principle to solar-cell analysis', *IEEE Transactions on Electron Devices*, vol. 26, pp. 165–171, 1979.

[38] M. Pilvet and M. Kauk-Kuusik, 'Study of Cu2(Zn,Cd)SnS4 Absorber Materials for Monograin Layer Solar Cells', Sep. 2017, Accessed: Apr. 01, 2022. [Online]. Available: https://digikogu.taltech.ee/et/Item/06aca692-ae00-4856-9312-46bc6ca7b2ad

[39] 'Quantum Efficiency | PVEducation'. https://www.pveducation.org/pvcdrom/solar-cell-operation/quantum-efficiency (accessed May 17, 2022).

[40] T. Raadik, N. Spalatu, J. Krustok, R. Josepson, and M. Grossberg, 'Temperature dependent optical and electrical characterization of SnS/CdS solar cell', *Thin Solid Films*, vol. 743, p. 139069, Feb. 2022, doi: 10.1016/j.tsf.2021.139069.